Homogenisation of sulphide inclusions within diamonds: A new approach to diamond inclusion geochemistry

Homogenisation of sulphide inclusions within diamonds: A new approach to diamond inclusion geochemistry

Iain McDonald[1]*, Hannah S. R. Hughes[2], Ian B. Butler[3], Jeffrey W. Harris[4], Duncan Muir[1]

[1]School of Earth and Ocean Sciences, Cardiff University, Park Place, Cardiff CF10 3AT, UK

[2]School of Geosciences, University of the Witwatersrand, Private Bag 3, Wits 2050, Johannesburg, South Africa

[3]School of Geosciences, University of Edinburgh, Edinburgh, EH9 3JW, UK

[4]School of Geographical and Earth Sciences, University of Glasgow, Glasgow, G12 8QQ, UK

*Corresponding author email: McDonaldi1@cf.ac.uk; Telephone: +44 (0)29 2087 4295

Submission to: ***Geochimica et Cosmochimica Acta***

Special issue from Highly Siderophile Elements workshop (Durham 2016)[1]

[1] **Abbreviations**: Platinum-group elements (PGE), Ir-group PGE (IPGE), Pd-group PGE (PPGE), monosulphide solid solution (Mss), intermediate solid solution (Iss)

Abstract

Base metal sulphide (BMS) inclusions in diamonds provide a unique insight into the chalcophile and highly siderophile element composition of the mantle. Entombed within their diamond hosts, these provide a more robust (closed system) sample, from which to determine the trace element, Re-Os and S-isotopic compositions of the mantle than mantle xenoliths or orogenic peridotites, as they are shielded from alteration during ascent to the Earth's crust, or and subsequent surface weathering. However, at temperatures below 1100^{o}C some BMS inclusions undergo subsolidus re-equilibration from an original monosulphide solid solution (Mss) and this causes fractionation of the major and trace elements within the inclusions. Thus to study the subjects noted above, current techniques require the *entire* BMS inclusion to be extracted for analyses. Unfortunately, 'flaking' of inclusions during break-out is a frequent occurrence and hence the risk of accidentally under-sampling a portion of the BMS inclusion is inherent in current practices. This loss, for example, may have significant implications for Re-Os isotopic analyses where incomplete sampling of a Re-rich phase, such as chalcopyrite, that typically occurs at the outer margins of BMS inclusions, may induce significant bias in the Re-Os and $^{187}Os/^{188}Os$ results, and therefore model and isochron ages.

We have developed a method for the homogenisation of BMS inclusions in diamond prior to their break-out from the host stone. Diamonds are heated to 1100^{o}C and then quenched ~~to~~ chemically homogenise any sulphide inclusions for both major and trace elements. Using X-ray Computed Microtomography (µCT) we determine the shape and spatial setting of multiple inclusions within a host stone and crucially show that the volume of a BMS inclusion is the same both before and after homogenisation. We show that the homogenisation process significantly reduces the inherent variability of *in situ* analysis when compared with unhomogenised BMS, considerably widening the scope for multiple methods of analysis, even on 'flakes' of single BMS inclusions. Finally we show that the trace elements present in peridotite (P-type) and eclogitic (E-type) BMS are distinct, with P-type diamonds having systematically higher total platinum-group element (particularly Os, Ir, Ru)

and Te and As concentrations. These distinctions suggest that the PGE and semi-metal budgets of mantle-derived partial melts may be significantly dependent upon the *type(s)* and proportions of sulphides present in the mantle source,

Keywords: Diamond, sulphide inclusion, homogenisation, PGE, Re-Os isotopes, semi-metals.

1. Introduction

Inclusions encapsulated within diamonds provide a rare opportunity to sample deep-seated mantle silicates, sulphides, fluids, metals or metal alloys. Diamonds are generally considered to be robust containers for these inclusions, effectively shielding them chemically during their ascent to the Earth's surface and preserving their composition. Inclusions are generally thought to have been formed syngenetically with the host diamond (as indicated by the imposed diamond morphology of the inclusions e.g.., Sobolev 1977, Meyer, 1987; Bulanova, 1995; Richardson et al., 2001; Richardson et al., 2004) and their study thus allows us an insight into mantle geochemistry, geodynamics, and diamond mineralisation processes that cannot be achieved by other means.

Base metal sulphides (BMS) are among the most common types of inclusion found in diamonds (e.g.. Harris and Gurney, 1979; Stachel and Harris, 2008) and occur in both major diamond parageneses, being relatively Ni-rich in peridotitic (P-type) diamond and relatively Ni-poor when associated with ecologitic (E-Type) diamonds. Their relative abundance may itself be informative about diamond mineralisation – transient volatile-rich (C, H, O, N, S) metasomatic agents have been suggested as key to diamond formation (e.g.., Deines and Harris, 1995; Westerlund *et al.,* 2004; Thomassot *et al.,* 2007 and 2009; Stachel & Luth, 2015). Thus studies of BMS inclusions within diamonds have become a major line of enquiry, both for the timing and genesis of diamond growth and for models of crustal and mantle development during the Archaean (e.g.., Hart *et al.*, 1997; Pearson *et al.,* 1998; Richardson *et al.,* 2001; Shirey *et al.*, 2004; Stachel and Harris, 2008; Richardson *et al.*, 2009; Harvey *et al.* 2016).

The first attempts to measure the trace element chemistry of whole diamonds containing BMS inclusions were made by Fesq *et al.*, (1973; 1975) using instrumental neutron activation analysis (INAA). They detected 40 trace elements, including Au and Ir, see below. With these early studies, however, instrumental limitations and lack of suitable standard materials meant that it was only in the 1990's that quantified concentrations of trace elements in inclusion-bearing whole diamonds

were first published (Schrauder *et al.*, 1996; Damarupurshad *et al.*, 1997; Hart *et al.*, 1997). In particular, Hart *et al.* (1997) noted a distinction between the Au/Ir ratios of P-type diamonds (Au/Ir <0.3) and E-type diamonds (Au/Ir ranging 0.3-100) and they linked this difference to protoliths involving melt-depleted cratonic mantle and subducted former oceanic lithosphere, respectively.

The INAA studies cited above involved analysis of whole diamonds, generally containing BMS and other inclusions, rather than BMS inclusions alone. The first attempt to analyse trace element concentrations in extracted BMS inclusions was made by McDonald *et al.* (1996) who dissolved extracted BMS and using inductively coupled plasma-mass spectrometry (ICP-MS). These authors determined the platinum-group elements (PGE), alongside Re and Au and the major elements (Fe, Ni, Cu), in two single inclusions and one composite sample (comprising multiple inclusions from the same stone), **extracted** from three Orapa E-type diamonds. Ruthenium, Rh, Pd and Au were measurable at ppm to 10's of ppm concentrations in both single inclusions and the composite sample but Ir, Pt and Re were below detection. Os was not analysed due to the volatilsation and loss of OsO_4 during the dissolution stage. In the same year Bulanova *et al.* (1996) analysed PGE and semi-metals at 10's-100's of ppm concentrations in BMS inclusions in Yakutian P-type and E-type diamonds by micro-PIXE (particle-induced X-ray emission) and found a strong enrichment in the Ir-group PGE (IPGE – Os, Ir and Ru) over the palladium-group PGE (PPGE – Rh, Pt and Pd).

Advances in laser ablation ICP-MS (LA-ICP-MS) and in the development of sulphide standards for *in situ* analysis of PGE and Au in BMS have led to rapid advances in the study of mantle sulphides (see recent reviews by Luguet and Reisberg, 2016; and Harvey *et al.*, 2016). But aside from work primarily devoted towards Re-Os isotopes there have been comparatively few studies devoted to analysing trace elements in diamond-hosted BMS since the 1990's. The work by Aulbach *et al.* (2012) on BMS in E-type diamonds from the Slave craton is the only recent study to provide comprehensive PGE, Au, Re and semi-metal data for diamond-hosted BMS inclusions.

This paucity of results may arise from the fact that the sulphides themselves present a number of problems for geochemical and isotopic investigations, stemming from the re-equilibration of high temperature monosulphide solid solution (Mss) to Fe-, Ni- and Cu-rich endmembers during cooling (Naldrett 1989; 2004; Taylor and Liu 2009). During this process (summarised in Figure 1) the PGE, Au, Re and semi-metals partition and fractionate between the different Fe-, Ni- and Cu-rich sulphide minerals and may also form discrete platinum-group minerals (PGM) or gold-rich minerals such as tellurides (e.g.. Fleet *et al*, 1993; Barnes *et al.*, 1997; Mungall *et al.*, 2005; Helmy *et al.*, 2007; Taylor and Liu 2009; Holwell and McDonald 2010). Because of this fractionation, it is incumbent that all of the mass of the inclusion be extracted intact to ensure a completely unbiased composition of the original bulk sulphide (Richardson *et al.*, 2001; Taylor and Liu 2009; Harvey *et al.* 2016). However, the 'flaking' or disintegration of the sulphide during inclusion extraction by breaking open the diamond, is a common and frequently documented inherent problem (e.g.., Deines & Harris, 1995; Pearson *et al.,* 1998; Richardson *et al.,* 2001; Thomassot *et al.,* 2009; Richardson *et al.*, 2009). Thus, partial sampling of BMS inclusions is common and may introduce a serious bias to geochemical and/or isotopic results and classifications. The partitioning studies cited above demonstrate that a fragment of the Cu-rich endmember of the fractionated inclusion will have significantly higher Re, Au, Pt and Pd and lower Ni, Ir, Os and Ru abundances than the Ni-rich counterpart from the same inclusion (and vice versa). Cu-rich sulphides are commonly observed to have exsolved to the edges of BMS inclusions and are therefore most susceptible to flaking and incomplete sampling when the diamond is broken.

The genesis ages of BMS inclusions in diamond have been determined as either model ages, or more commonly, as isochrons using Re-Os isotopic systematics (e.g. Pearson and Shirey, 1998; Stachel and Harris, 2008; and Harvey *et al.,* 2016). These results are also reliant upon measuring the *total* sulphide composition. Due to the intrinsically different compatibility of Re (into the Cu-rich endmember) from Os (into the Ni-Fe endmember) in the re-equilibrating sulphide (Figure 2), these elements may become significantly fractionated from one another. Further complications arise if Re

partitions into any PGM (e.g. Wainwright *et al.*, 2016). Fractionation may start at any time *after* the sulphide has been encapsulated in the diamond and the isotopic implications are dependent upon the timing and length of the fractionation. For example, the similar Os-isotopic composition ($^{187}Os/^{188}Os$ or expressed as γ_{Os}) of the core (Ni-(Os)-rich) *vs*. rim (Cu-(Re)-rich) of a differentiated sulphide inclusion from a single Kimberley diamond was used by Richardson *et al.,* (2001) to suggest that fractionation of the sulphide took place during, or just prior to, transport of the diamond to the surface in the Cretaceous (Richardson *et al.,* 2001). Whilst in this case, fractionation apparently had little effect on the Re-Os isotopic systematics of the inclusion, this may not be the case for inclusions that have been held at temperatures beneath the Mss liquidus for long periods of time, or especially for diamonds from geologically old kimberlites where BMS have fully fractionated and potential for in-growth of ^{187}Os into chalcopyrite is maximised. This potential sampling problem is inherent in all approaches that rely on unhomogenised sulphide inclusions regardless of whether fragments are analysed by wet chemistry or *in situ* by LA-ICP-MS.

Sulphur isotopic compositions (particularly $\delta^{34}S$) may also be affected by partial sampling of inclusions, as instrumental mass-fractionation is sensitive to the endmember sulphide analysed (e.g.., Chaussidon *et al.,* 1987; Thomassot *et al.,* 2009). Sulphide inclusions in Orapa diamonds show a range in $\delta^{34}S$ from +2.1 to +9.5‰ (pyrrhotite, Chaussidon *et al.,* 1987) to -11 to +2 ‰ (MSS and pyrrhotite, Eldridge *et al.,* 1991). More recently, a smaller range of pyrrhotite inclusion $\delta^{34}S$ compositions, from -1.4 to +2.6‰, has been reported by Farquhar *et al.* (2002). We note that the study by Farquhar *et al.* (2002) used inclusions with a smaller range in Ni-content, either suggesting that a subset of the Orapa sulphide population was represented in their 2002 study and/or that preceding studies could exemplify a degree of bias in sampling fragmented inclusions. Mass-independent fraction $\Delta^{33}S$ in the Farquhar *et al.* (2002) study reported a range from -0.1 to +0.6‰. In all cases, the range of $\delta^{34}S$ and $\Delta^{33}S$ has been used to infer an isotopic signature for both younger (< 2.45 Ga) and older (> 2.45 Ga) subduction of S-bearing sediments, as recorded in the mantle (e.g.., Farquhar *et al.,* 2002; Thomassot *et al.,* 2009).

In principle if the diamond remains a closed system then BMS inclusions could be homogenised (through a process of re-melting and rapid quenching) as part of the sample preparation *prior* to sulphide inclusion break-out from the diamond host. This would eliminate any partial sampling bias and effectively mean that any fragment of a homogenised inclusion is representative (geochemically and isotopically) to the total sulphide composition encased within the diamond originally. This process potentially provides a new and rigorous test of sulphide inclusion geochemical variability across diamond suites or in cases where there are multiple inclusions within a single diamond host crystal. In particular, it would provide a more robust sampling system for Re-Os isotopic analyses where accidental sampling bias (leading to the exclusion of Re and potentially ^{187}Os-rich chalcopyrite) may have detrimental effects on calculations of model ages and initial ratios (e.g. Richardson *et al.* 2001; Shirey *et al.*, 2013; Harvey *et al.*, 2016). The homogenisation method we describe below permits analysis of sulphide inclusions for both major elements by fully quantitative scanning electron microscopy (SEM) and energy dispersive spectrometry (EDS) and trace elements (by LA-ICP-MS) which allows use of the same inclusions for a full geochemical suite of elements, avoids any volatilisation problem of Os, and allows for direct calculation of S/metal and S/Se ratios pertinent to identifying if metal alloy phases are present within the sulphide (e.g.., Fleet *et al.,* 1991).

2. Diamond samples

The diamonds and BMS inclusions used in this study are from the Orapa kimberlite in NE Botswana, the mine being situated on the western edge of the Kaapvaal-Zimbabwe Craton (Kalahari Craton) within the 2.1-1.9 Ga Magondi orogenic belt (Fig. 3; Silver *et al.,* 2006 and references therein). The pipe has a Cretaceous eruption age of c. 93 Ma (Davis, 1977; Haggerty *et al.,* 1983). The genesis age of Orapa diamonds was first estimated to be 990 ± 50 Ma (based on a Nd/Sm isochron; Richardson, 1989) but more recently Ar-Ar dating of clinopyroxene inclusions have given genesis ages of 906-1032 Ma with a minor older group of diamonds at > 2500 Ma (Burgess *et al.,* 2004). Sulphide

inclusions from Orapa E-type diamonds have been dated (Re-Os model age) to include multiple ages of between 2.5-3.0 Ga and 1.0 Ga (see Shirey *et al.,* 2001; Shirey *et al.,* 2002 and references therein).

The sub-solidus sulphide mineralogy from Orapa inclusions in diamond has been previously reported by Deines & Harris (1995). From random polished sections, almost half of the 21 inclusions studied by these authors comprised only pyrrhotite (10). The remaining inclusions being monosulphide solid solution (4), a mixture of pyrrhotite and pentlandite (4), pyrrhotite-pentlandite-chalcopyrite (2) and pentlandite-chalcopyrite (1). Based on the Ni-content of the sulphides, approximately 85% of ~~diamonds~~ these inclusions from Orapa are thought to be from the eclogite paragenesis (on the basis of <8% Ni; Yefimova *et al.,* 1983).

Five colourless diamonds (see Table 1), each approximately 4mm in diameter and of 1 carat weight were used for experiments in this study. In all cases there were no fractures to the surface of the stones from the inclusions. Diamond H1 was a dodecahedral macle and its rounded surface prevented clear internal viewing, but a prominent black metallic rosette fracture within the central portion of the diamond was still visible. Diamond H2 was an elongate octahedron with negative trigons on many of the octahedral surfaces. At least four metallic rosette fractures were visible within this specimen, and the sulphide 'eyes' within these systems could be seen. Diamond H3 was a colourless well-shaped octahedron with slightly rounded edges and exhibiting negative trigons on most faces. Apart from a relatively large single sulphide rosette in the centre of the stone some smaller sulphides were noted in later analysis (see Fig. 7). Inclusion sizes ranged from about 50 to 200 microns. Diamond IM2 was a colourless broken dodecahedron and IM6 was a colourless elongate rounded octahedron. Based on external morphology, the diamonds showed no evidence of plastic deformation.

3. Experimental methods

The main aim of our experimental process is to heat all sulphide inclusion(s) within the diamond host to a temperature above the Mss liquidus (1100^{o}C – see for example Kullerud & Yoder, 1959; Arnold, 1971; Bowles *et al.,* 2011) allowing all sulphide phases to fully homogenise, and thereafter to quench the inclusion so rapidly that sulphide fractionation is minimised to the extent that the grain size is at or below the scale of sampling used by SEM or LA-ICP-MS. Thus the major and trace element composition of the sulphide inclusions are made uniform and any partial sample extracted from the diamond will be representative of the average composition of the inclusion (Fig. 2). This process is similar to that used for preparation of homogenised sulphide inclusions in chromitites by Holwell *et al.* (2011).

The homogenisation experiments were performed at the University of Edinburgh's (UK) Experimental Geoscience Facility. A vertical tube 1 atmosphere furnace was connected to H_2 and CO_2 gas supplies via Bronkhorst™ gas mass flow controllers to establish a defined fO_2 at the furnace hotspot. The hotspot temperature used was 1100^{o}C, and a gas mix of 14% H_2 and 86% CO_2 was used to ensure a calculated fO_2 environment between $10^{-11.3}$ to $10^{-11.4}$ (i.e., QFM-1 buffer; Deines *et al.,* 1974) to prevent the diamond from combusting and the sulphide inclusion from oxidising. Due to space restrictions within the tube furnace and the strict location of the 'hot spot' at the target temperature within it, each of the three diamonds to be homogenised were run separately through the experimental set-up. The diamond was suspended in a cradle of machinable alumina and Pt wire and positioned within the cold portion at the top of the tube furnace while the furnace was flushed with CO_2 gas. After flushing with CO_2, the CO_2/H_2 mix was allowed to stabilise for 5 minutes before the sample was lowered to the hot spot of the furnace. Based on the relative size of the diamonds compared with the 1 cm^3 chromitite blocks successfully homogenised by Holwell *et al.* (2011) each specimen was allowed to homogenise for 15 minutes. For rapid quenching, the Pt-wire hanger of the crucible was electrically fused, releasing the diamond (and cradle) to drop out of the furnace and into a cold water trap attached to the base of the tube furnace. Before recovery, the furnace was

205 flushed with pure CO_2 for 10 minutes to remove H_2 from the furnace before the quench trap was
206 removed.

207 The very different relative thermal expansion of diamond and the sulphide inclusion typically results
208 in a rosette fracture system being observed around BMS inclusions in diamond (Taylor and Liu 2009).
209 Whilst these fracture systems may further develop during heating, in the present cases, none were
210 sufficient to break the diamonds used in the experiments, thus the geochemical systems of the
211 sulphide inclusions were not compromised.

212 After homogenisation and quenching the faces of the diamonds showed nothing more than a mild
213 'frosting' effect. On diamond H1, these etch marks were distributed unevenly across the
214 crystallographic faces, principally because the diamond was a rounded dodecahedron, but for
215 diamond H2, an octahedron, the etching patterned showed positive trigons on octahedral faces. In
216 both cases, no surface graphite was noted. The surface etching is likely the result of the CO_2/H_2 gas
217 mix flowing through the furnace.

218

219 **4. Analytical techniques**

220 *4.1 X-ray Computed Microtomography (µCT)*

221 Tomographic data from diamond H3 (Table 1) was acquired before and after homogenisation using
222 the µCT instrument designed and built at the University of Edinburgh. The instrument comprised a
223 10-160kV Feinfocus transmission x-ray source, a MICOS UPR-160-Air rotary table and a Perkin Elmer
224 XRD0822 1 megapixel flat panel amorphous silicon detector with a Gd2O2S:Tb scintillator, operated
225 by control software developed in-house. For the whole diamond scan we used 600 projections and
226 the voxel size of the reconstructed data was 6.2 microns. For the inclusion scan we used 2000
227 projections and the voxel size was 2.0 microns. All scans were carried out at 100kV peak energy
228 using a 2 second exposure for each projection collected through a 360° sample rotation. The target

power was 2.7W. Tomographic slices were reconstructed by filtered back projection using Octopus 8.7 (Vlassenbroek et al., 2007) and visualised in 2D and 3D using Fiji and Avizo 9 software.

4.2 Sulphide inclusion recovery and preparation

Following homogenisation the sulphides were recovered from the diamond by standard break-out methods (Harris and Gurney 1979; Stachel and Harris 2008). The inclusions that had undergone experimental homogenisation were not recovered completely whole and broke during recovery. As such, a sub-selection of inclusions (listed in Table 1) were mounted in epoxy resin-filled stubs and polished to 0.25µm grade, using aluminium oxide polishing powder. The largest inclusions (whole or broken fragments) were preferentially chosen in order to test if the homogenisation was successful.

Unhomogenised sulphide inclusions IM2a, IM2b and IM6a that did not undergo this experimental procedure were used for comparison. The details of these inclusions can also be found in Table 1.

4.3 SEM imaging, element mapping and quantitative analysis

Backscattered electron (BSE) images were obtained for each inclusion studied using a Zeiss Sigma HD Scanning Electron Microscope at Cardiff University at operating conditions of 20 kV with ~ 1 nA beam current. Element mapping was performed using dual 150 mm^2 active area EDS detectors fitted to the SEM and Oxford Instruments Aztec software at operating conditions of 20 kV and ~ 2 nA. Maps were acquired with a step-size between 0.5 and 1 µm and a pixel dwell time of 15 to 20 ms at a working distance of 8.9 mm. Quantitative spot and area microanalyses were obtained using the same equipment with Co as a reference standard to measure beam drift every 15 minutes. Elements were calibrated prior to analysis with MicroAnalysis Consultants Ltd and Astimex Standards Ltd metal and mineral standards. Accuracy and precision of SEM chemical data was measured using

Astimex chalcopyrite and pentlandite standards (Supplementary Table A). Repeated spot analyses at the beginning and end of the analytical session demonstrate relative accuracies of 0.4-2.6% for S, 0.1-0.8% for Cu, 0.8-2.7% for Ni, 0.3-3.2% for Fe and 23-41% for Co (at a concentration of 0.43 wt%). 1σ precision on these repeated measurements was ≤0.23 wt% for S, ≤0.30 wt% for Fe, ≤0.11 wt% for Cu, 0.05 wt% for Co and 0.58 wt% for Ni respectively.

4.4 Laser ablation ICP-MS

Polished blocks were selected for laser ablation inductively coupled plasma mass spectrometry (LA-ICP-MS) for sulphide trace element analysis. Time resolved analysis (TRA) by LA-ICP-MS was performed on each BMS inclusion at Cardiff University on a New Wave Research UP213 UV laser system attached to a Thermo X Series 2 ICP-MS. Each inclusion underwent multiple analyses (by spots, lines, or both) to allow for data repeatability and homogeneity to be assessed. Both line and spot analysis were used and independently calibrated. For lines, a minimum length of ~80μm and a beam diameter of 40 μm were used, with laser operating conditions of 10 Hz frequency, 0.063 mJ at 4.98 Jcm^{-2} and sample translation at 6 μm sec^{-1}. For spot analysis, beam size was 40 μm and the same laser operating conditions as for the line analyses were employed. Acquisition times ranged 40 to 80 seconds with a gas blank measured for 20 seconds prior to laser ablation. Major element abundances (Fe, Ni, Cu, S) of the sulphide were measured by SEM-EDS (as outlined in section 6.3) prior to LA-ICP-MS, and ^{33}S was used as an internal standard for trace element calibration. Gas blank subtraction and internal standard corrections were carried out on Thermo Plasmalab software.

Five synthetic Ni-Fe-S quenched sulphide standards were used for LA-ICP-MS calibration, including S, Ni, Fe and Cu as major elements, and Co, As, Se, Ru, Rh, Pd, Ag, Cd, Sb, Te, Re, Os, Ir, Pt, Au and Bi as trace elements. The compositions and details of analytical methods for these standards are presented in Prichard *et al.* (2013) and further procedural details are available in Smith *et al.* (2014).

Standards 1-3 were used for calibration of Fe, Ni, Cu, Co, Zn and Cd as well as matrix-matched corrections for argide species, which interfere with light PGE isotopes ($^{59}Co^{40}Ar$, $^{61}Ni^{40}Ar$, $^{63}Cu^{40}Ar$, $^{65}Cu^{40}Ar$ and $^{66}Zn^{40}Ar$). Standard 1, containing 143 ppm Cd, was also used in corrections for ^{106}Cd on ^{106}Pd and ^{108}Cd on ^{108}Pd. Independent corrections for isotopes of the same element (e.g., $^{66}Zn^{40}Ar$ and ^{106}Cd on ^{106}Pd, and ^{108}Cd on ^{108}Pd) showed < 20% variance for Ru isotopes at concentrations from 0.1-0.2 ppm Ru and 3-10% for Pd isotopes at concentrations around 1 ppm Pd, indicating that the correction criteria are appropriate.

The accuracy for PGE and Au was checked by analysis of the Laflamme-Po724 standard as an unknown against the Cardiff quenched sulphide standards (results in Supplementary Material Table B). Based on the repeated spot and line analyses of each diamond sulphide inclusion (both from the homogenised and unhomogenised sample sets) 1σ precision can be calculated (Table 3). This shows 1σ precision to be typically 3-10% (concentrations 10-100 ppm), 4-41% (1-10 ppm) and 2-46% (<1 ppm) for homogenised samples. All LA-ICP-MS generated data are presented in Table 3, including argide and isobaric-corrected data with values displayed by isotope (for Ru, Rh and Pd).

5. Results

5.1 Sulphide inclusion recovery

Table 1 shows the recovery details of the larger sulphide inclusions recovered in this study. No *whole* inclusions were recovered from H1, but in total 5 large (> 100µm) and 10 small (< 100µm) pieces were obtained. These were grouped as one population initially. However, single inclusions typically produce 1-5 individual pieces on breakout and as the surface of H1 prevented clear viewing it is highly likely that this collection of fragments represents a mixture derived from a presently unknown number of multiple inclusions. On breakout, all four inclusions originally observed in H2 were recovered virtually whole and the two largest (H2a and H2b) were used for analysis. Diamond H3

shattered on breakout, flaking the one relatively large single inclusion in this stone and the largest fragment (H3a) from this was taken for analysis. Sulphide inclusion H2a (Table 1), had a visibly octahedral shape, imposed by the crystal structure of the diamond. Unhomogenised control diamond inclusions (IM2a, IM2b and IM6a) were recovered as fragments for comparison (Table 1). IM2a and IM2b were two pieces of an originally single inclusion from diamond IM2. IM6a was the largest fragment recovered from a single inclusion contained in stone IM6.

5.2 Petrography and major element mapping

Reflected light microscopy and back-scattered electron (BSE) images by SEM, per polished BMS inclusion, reveals a successful systematic homogenising effect for those diamonds that underwent the experimental heating and quenching process. As can be seen from the example shown in Figure 4a and 4b no zonation in endmember mineralogy can be identified under BSE above a grain size of <1 micron. On the other hand BSE images of unhomogenised samples display multiple sulphide mineral phases with distinct chalcopyrite-rich rims surrounding a pyrrhotite core, (Fig. 5a) or sub-solidus re-equilibration textures between pyrrhotite and pentlandite flames with isolated zones of chalcopyrite (Fig. 5b).

Element mapping (by SEM EDS) was also used to visualise the spatial distribution of Fe, Ni and Cu within each inclusion. Figures 6a and 6b show distinct zonation for Fe, Ni and Cu at scales of 25-300 microns in the unhomogenised samples. With exception of occasional single and multiple pixels that highlight very small (<1 up 3 microns wide) areas of Cu enrichment, but with insufficient Cu to be exsolved chalcopyrite, major elements are uniformly distributed throughout the homogenised inclusions (Figures 6c and 6d). No pixels indicating high concentrations of PGE, Re or Au that might represent sulphide containing PGM nanoparticles were observed.

5.3 Micro-CT visualisation

Figure 7 shows a 3D surface and volume rendering of the µCT data for diamond H3 which contained multiple sulphide inclusions (Fig. 7a), and volume renderings from discrete scans of the largest of these inclusions, before (Fig. 7b) and after (Fig. 7c) homogenisation. Whilst the diamond has a slightly rounded shape with negative trigons on the residual octahedral faces, the largest inclusion has a distinctive stepped shaped with faces in three inferred directions (x, y, z). This demonstrates that the sulphide inclusion has adopted a negative crystal shape from the diamond host. The definition of this stepped shape is very slightly more rounded for the inclusion *before* homogenisation (Fig. 7b), than *after* homogenisation (Fig. 7c), but this is likely to be an artefact of the resolution limit of the µCT data. For example, the apparent striations in Figure 7c can result from the slice structure of the tomographic data. Overall, the inclusion shape has been preserved in the homogenised sample indicating that none of the sulphide material was lost to fractures or mobilised elsewhere within the diamond.

To determine the volume of the inclusion *before* and *after* homogenisation, the non-local mean-filtered greyscale data were binarised using a global threshold in Avizo 9.2. The total volume of the inclusion was determined from the total voxels in the 3D volume of the binary image and the scan resolution. Before homogenisation the inclusion volume was estimated at 3.31×10^6 cubic microns. After homogenisation the inclusion volume was 3.28×10^6 cubic microns. Therefore the change in volumes before and after homogenisation are <1% which was within analytical error propagations.

Three-dimensional rotating movies of the diamond H3 and its inclusions within (both before and after homogenisation) are available in the online supplementary data files.

5.4 Major element geochemistry

Quantitative major element (S, Fe, Ni, Cu and Co) analyses (by quantitative EDS area analysis) were gathered for each inclusion (or inclusion fragment) for all homogenised and unhomogenised samples in this study (Table 2, *n = 142* – see Supplementary Figure A). These have been used to establish chemical variability either across single or fragmented sulphides, or between different sulphide fragments from within the same diamond, thereby allowing a quantitative comparison to be made between unhomogenised and homogenised samples. These data are shown in Figure 8 and a bar chart comparing S, Fe, Ni and Cu abundances by inclusion is given in Supplementary Table C.

The point analyses for the unhomogenised samples (*n* = 100) show a significant degree of variation between endmember compositions (Table 2, Fig. 8a-b). On a ternary Fe-Ni-S compositional diagram projected for a temperature of 1100^{o}C, these straddle the Mss, Mss + liquid, and liquid (L1) compositional fields (Fig. 8a), and equate to a continuum between pentlandite and pyrrhotite on the 100-135^{o}C diagram (Fig. 8b). Whilst the data closer to endmember pyrrhotite (Fig. 8b) have some Ni (up to a few wt%), for pentlandite many analyses plot as endmember compositions. A few analyses (2-5 point data) plot as mixtures between pentlandite and pyrrhotite (due to the spot size on the SEM overlapping fine pentlandite flames within Ni-bearing pyrrhotite). A single 'total' composition (by summing each pixel of the element mapping) based on the whole surface area of each unhomogenised inclusion exposed by polishing, was calculated using the INCA software and shows a representative total assumed composition for IM2 and IM6 (Fig. 8a-b). The calculated 'total' composition for IM2a and IM2b were indistinguishable and were therefore plotted as a single point on these diagrams. These equate to Ni-bearing pyrrhotite compositions akin to those plotted for the homogenised diamonds, but given the nature of the calculation, this alone cannot test the reproducibility of this method in estimating the total composition of an inclusion (as it is dependent upon a single exposed surface).

All analyses for the homogenised samples (*n = 42*) have a comparatively uniform major element composition (Table 2, Fig. 8c-d), with slight but systematic differences between inclusions from

different diamonds. Despite appearing homogenous under reflected light and BSE imaging, sulphides from diamond H1 divide into higher and lower Cu populations (H1a and H1c with 3.80 wt.% and H1b and H1d with 3.10 wt% Cu respectively) that likely reflect at least two different inclusions in the original stone (see Section 5.1). All the H1 sulphides have higher Cu contents and Ni contents than inclusions H2 and H3 (Table 2). In all inclusions analysed, however, the total Ni content was low enough to prescribe them as being E-type diamonds (< 8 wt.% Ni; Yefimova *et al.,* 1983, or < 15 wt.% Ni; Deines & Harris, 1995). All of the homogenised sulphide inclusions plot as Ni-bearing pyrrhotite on the ternary Fe-Ni-S compositional diagrams (Fig. 8c-d) and the compositional variation define a very tight data cluster of 42 points plotted on both Figures 8c and 8d. Any variation is unresolvable from the natural slight instrument divergence.

5.5 Trace element geochemistry

Representative time resolved analysis (TRA) plots from the LA-ICP-MS data for S, Fe, Ni, Cu and Co indicate that for all the unhomogenised samples, a distinct zonation is noted for major elements, particularly discernible for Cu, an example being shown in Figure 9a. In all the homogenised samples a zonation cannot be detected (e.g.., Fig. 9b). This lack of zonation in the homogenised sulphides extends to the trace elements where important elements like Re and, where measurable, Os can also be shown to exhibit near uniformity across a sulphide. For example, compare Figure 9c (unhomogenised) with Figure 9d (homogenised).These observations are true for both spot and line analyses by LA-ICP-MS. For the homogenised samples, both spot and line analyses give consistent calibrated element abundances (Table 3 and Supplementary Tables B, C and D). In Table 3 a comparison is given between unhomogenised and homogenised trace elements to 1σ values (per isotope analysed for each trace element).

6. Discussion

Before proceeding further it is important to demonstrate that homogenisation has been effective. The BSE-SEM images revealed no phase separation that could be identified above a grain size of <1 micron (Figure 4) and the element maps only highlighted anomalous Cu-rich pixels on a micron-scale. This is comparable or better than the sulphide homogenisation achieved by Holwell *et al.*, (2011). To further test the homogeneity of major and trace elements we have subdivided the TRA spectra obtained by LA-ICP-MS systematically into 5 second time blocks and determined the counts per second for Fe, Ni, Cu, Se, Ag, Te, Pd, Re, Pt and Au along with ratios (counts/counts) for Fe/Ni, Fe/Cu, Se/Ag, Se/Te, Pt/Pd, Re/Pt and Re/Au in each time block. From multiple time blocks we calculate a mean and standard deviation (1σ) and a relative standard deviation ((σ/mean) x 100%) to represent the variability across the data acquisition. This is shown graphically in Figure X and demonstrates an obvious reduction in variability on these ratios in the homogenised versus the unhomogenised inclusions regardless of whether spots or lines are used for analysis.

In Figures 10-16 we compare our Orapa sulphide inclusion trace element data with similar comprehensive trace element data for unhomogenised P-type sulphide inclusions from Yakutia (Siberian Craton) (Bulanova et al., 1996) and E-type sulphide inclusions from the Diavik Mine (Slave Craton; Aulbach et al., 2012). In addition, the present data **are** compared against documented Re and Os abundances, from E-type sulphides in diamonds from Jwaneng (Richardson et al., 2004), and Kimberley (Richardson et al., 2001), and from P- and E-type sulphide-bearing diamonds at Palmietgat (Simelane, 2004), and sulphides of unspecified paragenesis at Swartruggens (McKenna, 2001).

As with the major elements, TRA plots show significant variation in trace elements across single unhomogenised samples. For example, Figure 9c shows that Re and Au are notably enriched in the Cu-rich portions of the unhomogenised inclusions. By comparison, the homogenised inclusions (see Fig. 9d) shows no such peaked TRA signal for Re, Au or other trace elements. The metal/S ratios (metal = Fe+Ni+Cu) *vs.* PGE abundances, (see Fig. 10a), for all E-type diamonds (this study unhomogenised and homogenised, and similar data from Aulbach et al., 2012), range from 1.50 to

1.82, with total PGE abundances < 12ppm (Fig. 10a). The unhomogenised Orapa sulphide inclusions in that figure show a wide variation in metal/S ratio and total PGE, values reaching up to 1.75 and 8 ppm, with a broadly positive correlation that falls within the range previously documented for Diavik E-type diamonds by Aulbach et al. (2012). The homogenised Orapa inclusions by comparison have a very limited variability (on a diamond-by-diamond basis) giving distinct, but tightly clustering data, as seen in Figure 10a. Inclusions from homogenised diamond H1, for example, have 2-4ppm total PGE, an order of magnitude higher than the total PGE concentration of inclusions from diamonds H2 and H3 (0.2-0.4 ppm; see also Table 3). A similar situation exists between unhomogenised and homogenised sulphides if metal-to-metal ratios are compared to the PGEs, as shown in Figure 10b and 10c. In these two figures P-type sulphide data are added to allow a comparison with the earlier and present E-type data.

Chondrite normalised Ni-PGE-Au-Re-Cu diagrams (normalised after Fisher-Godde, 2010 for PGE and McDonough & Sun, 1995 for Ni, Re and Cu) are displayed in Figure 11. The grey background area delineates E-type inclusion compositions from Slave Craton diamonds; Aulbach et al., 2012). Overall, all analysed Orapa sulphide inclusions analysed have Ni-PGE-Au-Re-Cu patterns similar to those of Aulbach et al. (2012) with IPGE < PPGE. The unhomogenised Orapa inclusion patterns (Fig. 11a) show similar features to the homogenised ones (Fig. 11b), except that variation is minimised in the former. Per diamond, the systematic patterns of homogenised samples are distinct for diamond H1 relative to H2 and H3 (Fig. 11b). For example, Pt, Pd and Re are notably higher in inclusions from diamond H1, and these samples also have a distinctive negative Au anomaly. In comparison, inclusions from diamonds H2 and H3 have much lower Pt and Pd, slightly lower Os and Ir, a slight positive anomaly for Au and a slightly negative anomaly for Re (Fig. 11b). These apparent diamond-specific variations are not always reconcilable with the unhomogenised samples (Fig. 11a) because the variation from multiple analyses tends to make the pattern more scattered. However, we observed that unhomogenised samples from diamond IM6 have negative Au anomalies and generally the lowest Re concentrations (Fig. 11b). LA-ICP-MS analyses of unhomogenised samples with the highest Cu

447 component appear to have significantly higher Re contents, as well as higher Au, and PPGE (cf. Table
448 3; Fig. 11b). Also in Figure 11a, as a series of black crosses associated with some of the Ni-PGE-Au-
449 Re-Cu elements, are patterns for P-type diamonds from the Bulanova et al. (1996) study. These data
450 are clearly **distinct, with** enriched IPGE (such that IPGE > PPGE), higher Pd and generally lower Cu
451 contents than all the E-type diamonds.

452 The very low Os abundances in most of the unhomogenised Orapa sulphide inclusions (often < LOD),
453 contrasts with the extreme variation in Re (0.02 to 9.46 ppm Re; Table 3) in the same sulphide. This
454 relationship causes a spread of $(Re/Os)_N$ values for these samples and is shown in Figure 12a. By
455 contrast, the $(Re/Os)_N$ variability of homogenised samples, per diamond, is significantly reduced. This
456 variation in unhomogenised samples is proportional to the dominant end-member sulphide mineral
457 selectively sampled by the LA-ICP-MS, and in particular, the $(Re/Os)_N$ ratio is positively correlated
458 with the Cu content (Fig. 12b). Also, very low Ir abundances are observed for most of the analysed
459 Orapa sulphide inclusions (often < LOD), but again the extensive variation in Pd (0.07 to 2.39 ppm;
460 Table 3) in the unhomogenised samples causes a spread of $(Pd/Ir)_N$ for these samples (see Fig. 12c).
461 This variability is significantly reduced for the homogenised samples.

462 Figure 12d shows that the limited number of P-type sulphide-bearing diamonds analysed to date by
463 Bulanova *et al*., (1996) have very low $(Pd/Ir)_N$ relative to the E-type diamond dataset. This separation
464 is largely controlled by the high Ir contents of the P-type diamonds, and the low to very low (< LOD)
465 Pd contents. Consequently, the E- and P-type sulphide inclusions fall in distinct areas on $(Pd/Ir)_N$ *vs.*
466 $(Os/Ir)_N$ diagrams, (see Fig. 12d). More analyses of P-type sulphides from a greater number of
467 localities will be needed to establish the true extent of this separation.

468 Chondrite normalised (after McDonough & Sun, 1995) multi-element diagrams for semi-metals and
469 heavy metals are shown in Figure 13 (with the light grey area delineating the compositional range of
470 the E-type sulphide inclusions from Aulbach et al., 2012). Again, a greater variation in compositions
471 is seen for the unhomogenised samples in Figure 13a than for the homogenised Orapa inclusion

samples of Figure 13b. All E-type BMS inclusions observed have slight negative and slight positive anomalies for Te and Co, respectively, with unhomogenised samples having a particularly wide spread in Te abundance (Fig. 13a). All E-type BMS inclusions also have a notable negative As anomaly. Antimony, Ag, Cd and Bi are very variable between unhomogenised samples from different diamonds. For the homogenised diamond suite, H1 has the highest Bi content and generally (although not uniformly) the lowest Cd. Conversely, the P-type diamonds from the Bulanova study, shown as black crosses in Figure 13a are distinctive from the E-type compositions, with notably higher Te and As, and a great spread in Se abundances.

6. Wider implications

6.1 Comparisons with whole E-type diamonds and whole rock eclogites

Hart et al. (1997) determined Au and Ir concentrations in whole diamonds, with and without visible sulphide inclusions. Figure 14 shows that their E-type diamond data formed a steep and positively sloped array on a Au vs Ir plot with Au/Ir ratios > 0.3, whereas their P-type diamonds formed a flat or negatively sloped array with Au/Ir < 0.3. In both cases, absolute metal concentrations were very low (< 0.01 ppm) as the Au and Ir-bearing phases were diluted by the larger mass of the host diamond. The data generated in this present sulphide inclusion study and that of Aulbach et al. (2012) plot as an extension of the earlier E-type diamond Au vs Ir array in Figure 14 and may confirm that the Au and PGE concentrations in a whole diamond are probably controlled by small BMS inclusions. Such inclusions would be sub-microscopic in the case of diamonds that appear to be visually clear.

McDonald and Viljoen (2006) measured PGE and Au concentrations in whole rock samples of eclogites from Orapa and these are compared with alpine eclogites (Dale et al. 2009) and the homogenised BMS inclusions from this study on a chondrite normalised element plot in Figure 15. The whole rock Orapa eclogites show moderate fractionation of PPGE over IPGE and strong Cu

496 enrichment. Rhenium was not measured in the Orapa eclogite rocks but was in the alpine eclogites.
497 The alpine eclogites generally have lower PGE concentrations but similar pattern shapes to the
498 Orapa eclogites and also show a strong enrichment in Re. The metal concentrations of the E-type
499 sulphide inclusions are 2-3 orders of magnitude greater than the eclogite whole rock samples, but
500 they show similar PPGE:IPGE fractionation and the enrichment in Re and Cu observed in the whole
501 rocks. Comparison of the sulphide inclusion BMS to the bulk rock eclogite data suggests that the PGE
502 and Cu budget is largely controlled by the BMS compositions within the eclogites, however the Re
503 concentration in some of the diamond BMS inclusions is slightly lower than is predicted by the
504 eclogite bulk rock geochemistry. This may be specific to the diamond BMS inclusions analysed during
505 this study, or it may indicate a non-BMS Re-bearing phase present within the eclogite xenoliths but
506 absent in some of the diamond BMS inclusions (c.f. the Re present in the silicate fraction of
507 peridotite xenoliths; Handler and Bennett, 1999).

508

509 *6.2 Precious and semi-metal content of E-type vs P-type diamond sulphide inclusions*

510 The precious and semi-metal contents of E- and P-type diamond BMS inclusions appear to define
511 entirely distinct compositions. E-type BMS generally have low PGE abundances, with PPGE enriched
512 above IPGE, generally lower Se contents, and systematically lower Te and As concentrations than P-
513 type diamond BMS inclusions. E-type BMS also have higher metal/S ratios, lower Ni contents and
514 higher and/or more variable Cu contents. Re concentrations between E- and P-type BMS largely
515 overlap (e.g. Westerlund *et al.* 2006), however the notably higher Os abundance in P-type BMS
516 inclusions produces a significant difference in $(Re/Os)_N$ ratios.

517 Figure 16a shows that Te is higher in all P-type sulphide inclusions (Bulanova et al., 1996) than E-type
518 inclusions (this study and Aulbach et al., 2012) and there is a distinctive positive correlation between
519 Te and Se for P-type inclusions that is absent for E-type. P-type inclusions also have distinctly higher

520 Pd contents than E-type, such that the two populations of diamond inclusion types follow different
521 trends in Figure 16b (increasing Pd content with increasing Se for P-type inclusions only). Platinum
522 was generally < LOD in the Bulanova study and therefore we cannot compare Pt/Pd ratios for P- and
523 E-type inclusions, however we note that all E-type inclusions fall along a Pt:Pd line close to unity (Fig.
524 16c), and this trend is observed for inclusions from different host diamonds. Gold and Te do not
525 correlate with one another in the unhomogenised inclusions, nor in the dataset of Aulbach et al.
526 (2012), **see** (Fig. 16d). But when homogenised, 5 out of the 6 Orapa inclusions define positive a trend
527 between Au and Te. This suggests that Au and Te may be irregularly distributed within or between
528 sulphide minerals (possibly as alloys or micro-nuggets) that can be recombined by homogenisation.

529 In all diagrams in Figure 16, the homogenised inclusions form a tight cluster of compositions and
530 therefore are much less compositionally variable than analyses of the unhomogenised samples.
531 Whilst the homogenised inclusions tend to cluster per diamond host, we note that the two
532 inclusions from diamond H2 (which existed as two distinct inclusions within the diamond *before*
533 homogenisation, and remained as such *after* homogenisation) have different element
534 concentrations – inclusion H2a has higher Cu, Se, Re, Te and Pt contents than H2b (Fig. 16c) and this
535 is likely to be a primary feature inherited when each BMS inclusion was encapsulated. The same is
536 probably true for the fragments from diamond H1. H1a and H1c have higher Cu than H1b and H1d
537 (Table 2). The different S/Se ratios, Te, Au and Bi concentrations further suggest that each of the
538 large fragments represented by H1b, H1c and H1d originally came from separate inclusions rather
539 than one inclusion as originally suspected.

540 This intrinsic difference in E- and P-type diamond BMS inclusion metallogenic budgets may have
541 significant implications for the metallogenesis of the lithospheric mantle and/or the sources of
542 metals in mantle-derived melts (e.g.., Hughes *et al.,* 2015). Figures 11-13 reveal surprisingly close
543 similarities between the semi-metals present in E-type sulphides from Orapa and Diavik despite the
544 diamonds and sulphides forming on different cratons. This may reflect common protoliths or

processes operating during the formation of eclogites on the Slave and Kalahari cratons. Comparison of homogenised E- and P-type diamond BMS inclusions presents an opportunity to assess the wider metallogeny of the two main endmember lithologies of the mantle whilst removing uncertainties over secondary modification. Such studies may have major implications for the metal budget of mantle-derived melts in various tectonic environments through space and time.

7. Conclusions

- Heating diamonds (intact) with their inclusions in a furnace at 1100^{o}C, for 15 mins under controlled fO_2 conditions followed by quenching, successfully homogenises BMS inclusion(s), eradicating distinct endmember sulphide minerals (formed during natural cooling via subsolidus exsolution processes).
- µCT scanning of the diamond confirms that inclusions are the same volume (within error) both *before* and *after* homogenisation, demonstrating the success of this method. The diamond host retains each BMS inclusion with no loss or gain of inclusion material.
- µCT methods also gives an effective insight into the shape of BMS inclusions, including fracture propagation within diamond hosts. In this study, we observe a distinctive 3D stepped shape of a BMS inclusion and suggest this is in the form of a negative crystal shape, invoked by the diamond host.
- This homogenisation method produces BMS inclusions of a uniform geochemical composition for both major and trace elements (per inclusion). This has three implications:
    - Multiple geochemical analyses may now be carried out on homogeneous fragments of a single BMS inclusion, allowing for multiple interpretations to be made from a single diamond – for example, geochronology, isotopes and trace element analyses.

568 - Concerns regarding missing Re-rich mineral phases from unhomogenised BMS
569 inclusions (e.g.., by ‘flaking’ of chalcopyrite and accidental incomplete sampling of
570 whole inclusions) can be eradicated by utilising this homogenisation method.
571 - If multiple inclusions occur within a single diamond, each may be analysed
572 individually to assess spatial variation of BMS composition in a single diamond.
573 • Comparison of E-type diamond BMS inclusions in diamond to whole rock eclogite
574 compositions for PGE, Re, Au and Cu indicate that all metals (with the possible exception of
575 Re) are accounted for by the BMS.
576 • E-type and P-type diamond BMS inclusions in diamond have distinct trace element
577 signatures, especially for precious, heavy and semi-metals. P-type BMS inclusions have
578 higher total PGE and Te concentrations, higher IPGE (Os, Ir and Ru) and As abundances than
579 E-type BMS inclusions. This has important implications for the metallogeny of the mantle,
580 the partitioning behaviour of trace metals during partial melting, and the metal budgets that
581 may be imparted into mantle-derived magmas.

582

Acknowledgements

HSRH gratefully acknowledges her current Postdoctoral Fellowship with the Claude Leon Foundation and the support of the CIMERA centre of excellence at the Universities of the Witwatersrand and Johannesburg. The Diamond Trading Company (a member of the DeBeers Group of Companies) is thanked for the donation to JWH of the diamonds used in this study. The analytical work in this study was supported by NERC SoS Consortium grant NE/M011615/1 "Te and Se Cycling and Supply" awarded to Cardiff University.

591 **Figure Captions**

592 **Figure 1 –** Schematic timeline for the cooling and crystallisation of a sulphide liquid to monosulphide
593 solid solution (MSS), intermediate solid solution (ISS), a semimetal immiscible phase and low-
594 temperature mineral phases. Adapted from Holwell & McDonald (2010).

595 **Figure 2 –** Schematic diagram demonstrating the problems regarding partial sampling of a
596 fractionated (unhomogenised) sulphide inclusion and its apparent geochemistry *vs.* partial sampling
597 of a homogenised and quenched sulphide inclusion.

598 **Figure 3 –** Location map of Orapa, Magondi Belt and the Kaapvaal-Zimbabwe Craton. Adapted from
599 Shirey et al. (2001), McCourt et al. (2004) and Shirey et al. (2004).

600 **Figure 4 –** (a) Reflected light photomicrograph of homogenised inclusion H1d. (b) Back-scattered
601 electron (BSE) scanning electron microscope (SEM) image of homogenised inclusion H1d.
602 Abbreviations are pyrrhotite (Po), pentlandite (Pn), chalcopyrite (Cp) and monosulphide solid
603 solution (Mss).

604 **Figure 5 –** (a) Reflected light photomicrograph of unhomogenised inclusion IM2b. (b) BSE SEM image
605 of unhomogenised inclusion IM6a. Abbreviations are the same as in Figure 4.

606 **Figure 6 –** Combined element maps for Fe, Ni and Cu for (a) unhomogenised inclusion IM2b, (b)
607 unhomogenised inclusion IM6a, (c) homogenised inclusion H2a and (d) homogenised inclusion H3a.

608 **Figure 7 –** Micro-CT scan 3D rendered images for diamond H3 and its inclusions. (a) Diamond H3
609 itself shown as a semi-transparent blue shell with multiple sulphide inclusions as solid red shells. (b)
610 The largest of these sulphide inclusions in H3 before homogenisation and (c) the same inclusion
611 (from the same perspective) after homogenisation. See text for details.

Figure 8 – Ternary Fe-Ni-S diagrams for T = 1000°C and T = 100-135°C. Major element compositions (summarised in Table 2) for unhomogenised samples in (a) and (b). Major element compositions (summarised in Table 2) for homogenised samples in (c) and (d).

Figure 9 – Time resolved analyses (TRA) for two examples: Major element profiles for (a) an unhomogenised inclusion and (b) a homogenised inclusion. Example trace element profiles for (a) an unhomogenised inclusion and (b) a homogenised inclusion. See supplementary Tables D and E for all TRA plots for all diamond inclusion analyses.

Figure 10 – LA-ICP-MS data for homogenised and unhomogenised inclusions for (a) Metal/S ratio vs total PGE concentration, (b) Ni/(Ni+Fe+Cu) and (c) Cu/(Cu+Fe+Ni). Datasets from Bulanova et al. (1996) and Aulbach et al. (2012) for comparison.

Figure 11 – Multi-element diagrams for Ni, Cu, Re and the PGE: (a) shows unhomogenised samples and (b) shows homogenised samples. The light grey background delineates compositions from Aulbach et al. (2012) E-type Diavik diamond sulphide inclusions while the dashed lines indicate P-type diamond compositions from Yakutia by Bulanova et al. (1996). Downward arrows denote measurements where concentration was < LOD, and which have then been plotted at ½ LOD.

Figure 12 – LA-ICP-MS data for homogenised and unhomogenised inclusions for (a) $(Re/Os)_N$ vs Os, (b) $(Re/Os)_N$ vs Cu, (c) $(Pd/Ir)_N$ vs Ir and (d) $(Pd/Ir)_N$ vs $(Os/Ir)_N$. Downward arrows denote measurements where concentration was < LOD, and which have then been used at ½ LOD for calculated ratios for plotting.

Figure 13 – Multi-element diagrams for semi-metals and heavy metals: (a) shows unhomogenised samples and (b) shows homogenised samples. The light grey background delineates compositions from Aulbach et al. (2012) E-type Diavik diamond sulphide inclusions while the dashed lines indicate P-type diamond compositions from Yakutia by Bulanova et al. (1996). The order of elements in these

diagrams is based on those displayed by Aulbach et al., 2012. Downward arrows denote measurements where concentration was < LOD, and which have then been plotted at ½ LOD.

Figure 14 – Au vs Ir, after Hart *et al.* (1997).

Figure 15 – Multi-element diagrams for Ni, Cu, Re and the PGE comparing homogenised diamond inclusion samples with bulk rock data for eclogite xenoliths, abbreviated 'xnl', from Orapa McDonald et al. (2006) and for Alpine eclogites from the study by Dale et al. (2009).

Figure 16 – LA-ICP-MS data for homogenised and unhomogenised inclusions for (a) Te vs Se, (b) Pd vs Se, (c) Pt vs Pd and (d) Au vs Te.

Table Captions

Table 1 – List of homogenised and unhomogenised diamond samples and their sulphide inclusions, including dimensions of inclusions and fragments.

Table 2 – Summary table of the major element compositions of homogenised and unhomogenised diamond inclusion samples. Data are from SEM EDS. Refer to supplementary Table C for all point analyses and supplementary Figure A for a bar chart displaying data from Table 2.

Table 3 – Summary table of all trace element data (from LA-ICP-MS) of homogenised and unhomogenised diamond inclusion samples. See main text for details regarding calibration and argide corrections. Refer to supplementary Table B for all data (including all analysed isotopes) and supplementary Tables D and E for all TRA diagrams per analysis.

655 **References**

656 Agrosì, G., Nestola, F., Tempesta, G., Bruno, M., Scandale, E. and Harris, J., 2016. X-ray tomographic
657 study of a diamond from Udachnaya: Implications for the genetic nature of inclusions. Lithos,
658 248, pp.153-159.

659 Alard, O., Griffin, W. L., Lorand, J. -P., Jackson, S. E. & O'Reilly, S. Y. 2000. Non-chondritic distribution
660 of the highly siderophile elements in mantle sulphides. Nature, 407, 891-894.

661 Alard, O., Griffin, W.L., Pearson, N.J., Lorand, J.P. and O'Reilly, S.Y., 2002. New insights into the Re–
662 Os systematics of sub-continental lithospheric mantle from in situ analysis of sulphides. Earth
663 and Planetary Science Letters, 203(2), pp.651-663.

664 Arnold, R.G., 1971. Evidence for liquid immiscibility in the system FeS-S. Economic Geology, 66(8),
665 pp.1121-1130.

666 Aulbach, S., Griffin, W. L., Pearson, N. J., O'Reilly, S. Y., Kivi, K. & Doyle, B. J. 2004. Mantle formation
667 and evolution, Slave Craton: constraints from HSE abundances and Re–Os isotope systematics
668 of sulfide inclusions in mantle xenocrysts. Chemical Geology, 208, 61-88.

669 Aulbach, S., Stachel, T., Seitz, H.M. and Brey, G.P., 2012. Chalcophile and siderophile elements in
670 sulphide inclusions in eclogitic diamonds and metal cycling in a Paleoproterozoic subduction
671 zone. Geochimica et Cosmochimica Acta, 93, pp.278-299.

672 Barnes, S.J., Makovicky, E., Makovicky, M., Rose-Hansen, J. and Karup-Moller, S., 1997. Partition
673 coefficients for Ni, Cu, Pd, Pt, Rh, and Ir between monosulfide solid solution and sulfide liquid
674 and the formation of compositionally zoned Ni-Cu sulfide bodies by fractional crystallization of
675 sulfide liquid. Canadian Journal of Earth Sciences, 34(4), pp.366-374.

676 Bowles, J. F. W., Howie, R. A., Vaughan, D. J. & Zussman, J. (2011). Rock-forming inerals: Non-
677 silicates; Oxides, Hydroxides and Sulphides. Geological Society.

678 Bulanova, G.P., 1995. The formation of diamond. Journal of Geochemical Exploration, 53(1), pp.1-23.

679 Bulanova, G.P., Griffin, W.L., Ryan, C.G., Shestakova, O.Y. and Barnes, S.J., 1996. Trace elements in
680 sulfide inclusions from Yakutian diamonds. Contributions to Mineralogy and Petrology, 124(2),
681 pp.111-125.

682 Burgess, R., Kiviets, G.B. and Harris, J.W., 2004. Ar–Ar age determinations of eclogitic clinopyroxene
683 and garnet inclusions in diamonds from the Venetia and Orapa kimberlites. Lithos, 77(1),
684 pp.113-124.

685 Burton, K.W., Schiano, P., Birck, J.L. and Allegre, C.J., 1998. The behaviour of Re and Os in mantle
686 minerals with the implications for mantle melting EOS transaction. American Geophysical
687 Union, 79(46), S373.

688 Carlson, R.W., 2005. Application of the Pt–Re–Os isotopic systems to mantle geochemistry and
689 geochronology. Lithos, 82(3), pp.249-272.

690 Carlson, W.D., Denison, C. and Ketcham, R.A., 2000. High-resolution X-ray computed tomography as
691 a tool for visualization and quantitative analysis of igneous textures in three dimensions. Visual
692 Geosciences, 4(3), 1-14.

693 Chase, M.W., Jr., 1998. NIST-JANAF Themochemical Tables, Fourth Edition, J. Phys. Chem. Ref. Data,
694 Monograph 9, 1-1951.

695 Chaussidon, M., Albarede, F. and Sheppard, M.F., 1987. Sulphur isotope heterogeneity in the mantle
696 from ion microprobe measurements of sulphide inclusions in diamonds. Nature, 330, pp.242-
697 244.

698 Dale, C.W., Burton, K.W., Pearson, D.G., Gannoun, A., Alard, O., Argles, T.W. and Parkinson, I.J.,
699 2009. Highly siderophile element behaviour accompanying subduction of oceanic crust: whole
700 rock and mineral-scale insights from a high-pressure terrain. Geochimica et Cosmochimica Acta,
701 73(5), pp.1394-1416.

702 Damarupurshad, A., Hart, R., Sellschop, J. and Meyer, H., 1997. The application of INAA to the
703 geochemical analysis of single diamonds. Journal of radioanalytical and nuclear chemistry,
704 219(1), pp.33-39.

705 Davis, D.L. 1977. The ages and Uranium contents from Kimberlites and associated rocks. Extended
706 abstracts of the second International Kimberlite Conference, Santa Fe.

707 Deines, P. and Harris, J.W., 1995. Sulfide inclusion chemistry and carbon isotopes of African
708 diamonds. Geochimica et Cosmochimica Acta, 59(15), pp.3173-3188.

709 Denison, C. and Carlson, W.D., 1997. Three-dimensional quantitative textural analysis of
710 metamorphic rocks using high-resolution computed X-ray tomography: Part II. Application to
711 natural samples. Journal of Metamorphic Geology, 15(1), 45-57.

712 Eldridge, C.S., Compston, W., Williams, I.S., Harris, J.W. and Bristow, J.W., 1991. Isotope evidence for
713 the involvement of recycled sediments in diamond formation. Nature, 353(6345), pp.649-653.

714 Farquhar, J., Wing, B.A., McKeegan, K.D., Harris, J.W., Cartigny, P. and Thiemens, M.H., 2002. Mass-
715 independent sulfur of inclusions in diamond and sulfur recycling on early Earth. Science,
716 298(5602), pp.2369-2372.

717 Fesq, H., Bibby, D., Sellschop, J. and Watterson, J., 1973. The determination of trace-element
718 impurities in natural diamonds by instrumental neutron activation analysis. Journal of
719 Radioanalytical and Nuclear Chemistry, 17(1-2), pp.195-216.

720 Fesq, H.W., Bibby, D.M., Erasmus, C.S., Kable, E.J.D. and Sellschop, J.P.F., 1975. A comparative trace
721 element study of diamonds from Premier, Finsch and Jagersfontein mines, South Africa. Physics
722 and Chemistry of the Earth, 9, pp.817-836.

723 Fleet, M.E., Stone, W.E. and Crocket, J.H., 1991. Partitioning of palladium, iridium, and platinum
724 between sulfide liquid and basalt melt: Effects of melt composition, concentration, and oxygen
725 fugacity. Geochimica et Cosmochimica Acta, 55(9), pp.2545-2554.

726 Fleet, M.E., Chryssoulis, S.L., Stone, W.E. and Weisener, C.G., 1993. Partitioning of platinum-group
727 elements and Au in the Fe− Ni− Cu− S system: experiments on the fractional crystallization of
728 sulfide melt. Contributions to Mineralogy and Petrology, 115(1), pp.36-44.

729 Godel, B., 2013. High-resolution X-ray computed tomography and its application to ore deposits:
730 From data acquisition to quantitative three-dimensional measurements with case studies from
731 Ni-Cu-PGE deposits. Economic Geology, 108(8), 2005-2019.

732 Godel, B., Barnes, S.J. and Maier, W.D., 2006. 3-D distribution of sulphide minerals in the Merensky
733 Reef (Bushveld Complex, South Africa) and the JM Reef (Stillwater Complex, USA) and their
734 relationship to microstructures using X-ray computed tomography. Journal of Petrology, 47(9),
735 1853-1872.

736 Gréau, Y., Alard, O., Griffin, W.L., Huang, J.X. and O'Reilly, S.Y., 2013. Sulfides and chalcophile
737 elements in Roberts Victor eclogites: unravelling a sulfide-rich metasomatic event. Chemical
738 Geology, 354, pp.73-92.

739 Gréau, Y., Griffin, W.L., Alard, O. and O'Reilly, S.Y., 2008. Petrology and geochemistry of eclogitic
740 sulfides: a new insight on the origin of mantle eclogites. In 9th International Kimberlite
741 Conference.

742 Gréau, Y., Alard, O., Griffin, W.L., Huang, J-X., and O'Reilly, S.Y., 2013. Sulfides and chalcophile
743 elements in Roberts Victor eclogites: unravelling a sulphide-rich metasomatic event. Chemical
744 Geology, 354, 73-92.

745 Guo, J., Griffin, W. L. & O'Reilly, S. Y. 1999. Geochemistry and origin of sulphide minerals in mantle
746 xenoliths: Qilin, Southeastern China. Journal of Petrology, 40, 1125-1149.

747 Haggerty, S.E., Raber, E. and Naeser, C.W., 1983. Fission track dating of kimberlitic zircons. Earth and
748 Planetary Science Letters, 63(1), pp.41-50.

749 Handler, M.R., and Bennett, V.C., 1999. Behaviour of Platinum-group elements in the subcontinental
750 mantle of eastern Australia during variable metasomatism and melt depletion. Geochmica et
751 Cosmochimica Acta, 63, 3597-3618.

752 Harris, J. and Gurney, J.J., 1979. Inclusions in diamond. The properties of diamond, pp.555-591.

753 Hart, R.J., Tredoux, M. and de Wit, M.J., 1997. Refractory trace elements in diamond inclusions:
754 further clues to the origins of the ancient cratons. Geology, 25(12), pp.1143-1146.

755 Harvey, J., Warren, J.M. and Shirey, S.B., 2016. Mantle sulfides and their role in Re-Os and Pb isotope
756 geochronology. Reviews in Mineralogy and Geochemistry, 81(1), pp.579-649.

757 Helmy, H.M., Ballhaus, C., Berndt, J., Bockrath, C. and Wohlgemuth-Ueberwasser, C., 2007.
758 Formation of Pt, Pd and Ni tellurides: experiments in sulfide–telluride systems. Contributions to
759 Mineralogy and Petrology, 153(5), pp.577-591.

760 Holwell, D.A. and McDonald, I., 2010. A review of the behaviour of platinum group elements within
761 natural magmatic sulfide ore systems. Platinum Metals Review, 54(1), pp.26-36.

762 Holwell, D.A., McDonald, I. and Butler, I.B., 2011. Precious metal enrichment in the Platreef,
763 Bushveld Complex, South Africa: evidence from homogenized magmatic sulfide melt inclusions.
764 Contributions to Mineralogy and Petrology, 161(6), pp.1011-1026.

765 Howarth, G.H., Sobolev, N.V., Pernet-Fisher, J.F., Ketcham, R.A., Maisano, J.A., Pokhilenko, L.N.,
766 Taylor, D. and Taylor, L.A., 2015. 3-D X-ray tomography of diamondiferous mantle eclogite
767 xenoliths, Siberia: A review. Journal of Asian Earth Sciences, 101, pp.39-67.

768 Hughes, H.S., McDonald, I. and Kerr, A.C., 2015. Platinum-group element signatures in the North
769 Atlantic Igneous Province: Implications for mantle controls on metal budgets during continental
770 breakup. Lithos, 233, pp.89-110.

771 Hughes, H.S., McDonald, I., Loocke, M., Butler, I.B., Upton, B.G. and Faithfull, J.W., 2016. Paradoxical
772 co-existing base metal sulphides in the mantle: The multi-event record preserved in Loch Roag
773 peridotite xenoliths, North Atlantic Craton. Lithos.

774 Jacob, D.E., Wirth, R., Enzmann, F., Kronz, A. and Schreiber, A., 2011. Nano-inclusion suite and high
775 resolution micro-computed-tomography of polycrystalline diamond (framesite) from Orapa,
776 Botswana. Earth and Planetary Science Letters, 308(3), pp.307-316.

777 Ketcham, R.A. and Carlson, W.D., 2001. Acquisition, optimization and interpretation of X-ray
778 computed tomographic imagery: applications to the geosciences. Computers & Geosciences,
779 27(4), 381-400.

780 Ketcham, R.A. and Carlson, W.D., 2001. Acquisition, optimization and interpretation of X-ray
781 computed tomographic imagery: applications to the geosciences. Computers & Geosciences,
782 27(4), 381-400.

783 König, S., Luguet, A., Lorand, J.P., Wombacher, F. and Lissner, M., 2012. Selenium and tellurium
784 systematics of the Earth's mantle from high precision analyses of ultra-depleted orogenic
785 peridotites. Geochimica et Cosmochimica Acta, 86, pp.354-366.

786 Kullerud, G. and Yoder, H.S., 1959. Pyrite stability relations in the Fe-S system. Economic Geology,
787 54(4), pp.533-572.

788 Kyle J. R., Ketcham R. A., Mote A. S. Contributions of high resolution X-ray computed tomography to
789 ores studies. In: Muhling J., editor. Extended Abstracts, Predictive Mineral Discovery Under
790 Cover. Perth: University of Western Australia; 2004. p. 387-390.

791 Kyle, J.R. and Ketcham, R.A., 2003. In situ distribution of gold in ores using high-resolution X-ray
792 computed tomography. Economic Geology, 98(8), 1697-1701.

793 Lorand, J. -P. & Alard, O. 2001. Platinum-group element abundances in the upper mantle: New
794 constraints for in situ and whole-rock analyses of Massif Central xenoliths (France). Geochimica
795 et Cosmochimica Acta, 65, 2789-2806.

796 Lorand, J. -P., Alard, O., Luguet, A. & Keays, R. R. 2003. Sulfur and selenium systematics of the
797 subcontinental lithospheric mantle: Inferences from the Massif Central xenolith suite (France).
798 Geochimica et Cosmochimica Acta, 67, 4137-4151

799 Lorand, J. -P., Luguet, A. & Alard, O. 2013. Platinum-group element systematics and petrogenetic
800 processing of the continental upper mantle: A review. Lithos, 164-167, 2-21.

801 Luguet, A., Alard, O., Lorand, J.P., Pearson, N.J., Ryan, C. and O'Reilly, S.Y., 2001. Laser-ablation
802 microprobe (LAM)-ICPMS unravels the highly siderophile element geochemistry of the oceanic
803 mantle. Earth and Planetary Science Letters, 189(3), pp.285-294.

804 Luguet, A. & Reisberg, L., 2016. Highly Siderophile Element and ^{187}Os Signatures in Non-cratonic
805 Basalt-hosted Peridotite Xenoliths: Unravelling the Origin and Evolution of the Post-Archean
806 Lithospheric Mantle. Reviews in Mineralogy and Geochemistry, 81(1), 305-367.

807 McDonald, I., Harris, J.W. and Vaughan, D.J., 1996. Determination of noble metals in sulphide
808 inclusions from diamonds using inductively coupled plasma-mass spectrometry. Analytica
809 chimica acta, 333(1), pp.41-49.

810 McKenna, N., 2001. A study of the diamonds, diamond inclusion minerals and other mantle minerals
811 from the Swartruggens kimberlite, South Africa. MSc thesis, University of Cape Town, 226 pp.

812 Mees, F., Swennen, R., Van Geet, M. and Jacobs, P., 2003. Applications of X-ray computed
813 tomography in the geosciences. Geological Society, London, Special Publications, 215(1), 1-6.

814 Meyer, H.O., 1987. Inclusions in diamond. Mantle xenoliths, 1, pp.501-522.

815 Mungall, J.E., Andrews, D.R., Cabri, L.J., Sylvester, P.J. and Tubrett, M., 2005. Partitioning of Cu, Ni,
816 Au, and platinum-group elements between monosulfide solid solution and sulfide melt under
817 controlled oxygen and sulfur fugacities. Geochimica et Cosmochimica Acta, 69(17), pp.4349-
818 4360.

819 Naldrett, A.J., 1989. Sulfide melts; crystallization temperatures, solubilities in silicate melts, and Fe,
820 Ni, and Cu partitioning between basaltic magmas and olivine. Reviews in Economic Geology, 4,
821 pp.5-20.

822 Naldrett, A.J., 2011. Fundamentals of magmatic sulfide deposits. Reviews in Economic Geology, 17,
823 pp.1-50.

824 Palyanov, Y.N., Borzdov, Y.M., Khokhryakov, A.F., Kupriyanov, I.N. and Sobolev, N.V., 2006. Sulfide
825 melts–graphite interaction at HPHT conditions: implications for diamond genesis. Earth and
826 Planetary Science Letters, 250(1), pp.269-280.

827 Pearson, D.G., Shirey, S.B., Harris, J.W. and Carlson, R.W., 1998. Sulphide inclusions in diamonds
828 from the Koffiefontein kimberlite, S Africa: constraints on diamond ages and mantle Re–Os
829 systematics. Earth and Planetary Science Letters, 160(3), pp.311-326.

830 Pearson, D.G., Shirey, S.B., Harris, J.W. and Carlson, R.W., 1998. Sulphide inclusions in diamonds
831 from the Koffiefontein kimberlite, S Africa: constraints on diamond ages and mantle Re–Os
832 systematics. Earth and Planetary Science Letters, 160(3), pp.311-326.

833 Pearson, N.J., Alard, O., Griffin, W.L., Jackson, S.E. and O'Reilly, S.Y., 2002. In situ measurement of
834 Re-Os isotopes in mantle sulfides by laser ablation multicollector-inductively coupled plasma

mass spectrometry: analytical methods and preliminary results. Geochimica et Cosmochimica Acta, 66(6), pp.1037-1050.

Prichard, H. M., Knight, R. D., Fisher, P. C., McDonald, I., Zhu, M. -F. & Wang, C. Y. 2013. Distribution of platinum-group elements in magmatic and altered ores in the Jinchuan intrusion, China: an example of selenium remobilization by postmagmatic fluids. Mineralium Deposita, 48, 767-786.

Reisberg, L. and Meisel, T., 2002. The Re-Os Isotopic System: A Review of Analytical Techniques. Geostandards Newsletter, 26(3), pp.249-267.

Richardson, S.H., Shirey, S.B., Harris, J.W. and Carlson, R.W., 2001. Archean subduction recorded by Re–Os isotopes in eclogitic sulfide inclusions in Kimberley diamonds. Earth and Planetary Science Letters, 191(3), pp.257-266.

Richardson, S.H., Shirey, S.B. and Harris, J.W., 2004. Episodic diamond genesis at Jwaneng, Botswana, and implications for Kaapvaal craton evolution. Lithos, 77(1), pp.143-154.

Richardson, S.H., Pöml, P.F., Shirey, S.B. and Harris, J.W., 2009. Age and origin of peridotitic diamonds from Venetia, Limpopo Belt, Kaapvaal–Zimbabwe craton. Lithos, 112, pp.785-792.

Richardsons. H. (1989) Radiogenic isotope studies of diamond inclusions. 28th Intl. Geol. Congress, Workshop on Diamonds. Extended Abstracts, pp. 87-90.

Saunders, J.E., Pearson, N.J., O'Reilly, S.Y. and Griffin, W.L., 2015. Sulfide metasomatism and the mobility of gold in the lithospheric mantle. Chemical Geology, 410, 149-161.

Schrauder, M., Koeberl, C. and Navon, O., 1996. Trace element analyses of fluid-bearing diamonds from Jwaneng, Botswana. Geochimica et Cosmochimica Acta, 60(23), pp.4711-4724.

Schulze, D.J., Wiese, D. and Steude, J., 1996. Abundance and distribution of diamonds in eclogite revealed by volume visualization of CT X-ray scans. The Journal of Geology, 104, 109-114.

Shirey, S.B. and Walker, R.J., 1995. Carius tube digestion for low-blank rhenium-osmium analysis. Analytical Chemistry, 67(13), pp.2136-2141.

Shirey, S.B., Carlson, R.W., Richardson, S.H., Menzies, A., Gurney, J.J., Pearson, D.G., Harris, J.W. and Wiechert, U., 2001. Archean emplacement of eclogitic components into the lithospheric mantle during formation of the Kaapvaal Craton. Geophysical Research Letters, 28(13), pp.2509-2512.

Shirey, S.B., Harris, J.W., Richardson, S.H., Fouch, M.J., James, D.E., Cartigny, P., Deines, P. and Viljoen, F., 2002. Diamond genesis, seismic structure, and evolution of the Kaapvaal-Zimbabwe craton. Science, 297(5587), pp.1683-1686.

Shirey, S.B., Richardson, S.H. and Harris, J.W., 2004. Integrated models of diamond formation and craton evolution. Lithos, 77(1), pp.923-944.

Shirey, S.B., Cartigny, P., Frost, D.J., Keshav, S., Nestola, F., Nimis, P., Pearson, D.G., Sobolev, N.V. and Walter, M.J., 2013. Diamonds and the geology of mantle carbon. Reviews in Mineralogy and Geochemistry, 75(1), pp.355-421.

870 Silver, P.G., Fouch, M.J., Gao, S.S. and Schmitz, M., 2004. Seismic anisotropy, mantle fabric, and the
871 magmatic evolution of Precambrian southern Africa. South African Journal of Geology, 107(1-2),
872 pp.45-58.

873 Simelane, V.G., 2004. Palmietgat kimberlite pipes, **South** Africa: Clues to the nature and origin of the
874 sub-Bushveld Kaapvaal Craton. University of the Witwatersrand, MSc thesis.

875 Smith, J. W., Holwell, D. A. & McDonald, I. 2014. Precious and base metal geochemistry and
876 mineralogy of the Grasvally Norite-Pyroxenite-Anothosite (GNPA) member, northern Bushveld
877 Complex, South Africa: implications for a multistage emplacement. Mineralium Deposita, 49,
878 667-692.

879 Sobolev, N.V., 1977. Deep-Seated Inclusions in Kimberlites and the Problem of the Composition of
880 the Upper Mantle. American Geophysical Union. pp. 83-153.

881 Sobolev, N.V., Yefimova, E.S. and Usova, L.V., 1983. Eclogitic paragenesis of diamonds from the Mir
882 kimberlite pipe. Mantle xenoliths and problems of ultrabasic magmas, pp.4-16.

883 Stachel, T. and Harris, J.W., 2008. The origin of cratonic diamonds—constraints from mineral
884 inclusions. Ore Geology Reviews, 34(1), pp.5-32.

885 Stachel, T. and Luth, R.W., 2015. Diamond formation—Where, when and how?. Lithos, 220, pp.200-
886 220.

887 Taylor, L.A., and Liu, Y., 2009. Sulfide inclusions in diamonds: not monosulfide solid solution. Russian
888 Geology and Geophysics, 50, 1201-1211.

889 Thomassot, E., Cartigny, P., Harris, J.W. and Viljoen, K.F., 2007. Methane-related diamond
890 crystallization in the Earth's mantle: stable isotope evidences from a single diamond-bearing
891 xenolith. Earth and Planetary Science Letters, 257(3), pp.362-371.

892 Thomassot, E., Cartigny, P., Harris, J.W., Lorand, J.P., Rollion-Bard, C. and Chaussidon, M., 2009.
893 Metasomatic diamond growth: A multi-isotope study (13C, 15N, 33S, 34S) of sulphide inclusions
894 and their host diamonds from Jwaneng (Botswana). Earth and Planetary Science Letters, 282(1),
895 pp.79-90.

896 Victor, A.C. 1962. Heat Capacity of Diamond at High Temperatures. The Journal of Chemical Physics,
897 36 (7), pp. 1903-1911.

898 Vlassenbroeck, J., Dierick, M., Masschaele, B., Cnudde, V., Van Hoorebeke, L., Jacobs, P., 2007.
899 Software tools for quantification of X-ray microtomography at the UGCT. Nuclear Instruments
900 and Methods in Physics Research A 580 (1), 442–445.

901 Welke, H.J., Allsopp, H.L., and Harris, J.W., 1974. Measurements of K, Rb, U, Sr and Pb in diamonds
902 containing inclusions. Nature, 252, pp.35-37.

903 Westerlund, K.J., Gurney, J.J., Carlson, R.W., Shirey, S.B., Hauri, E.H. and Richardson, S.H., 2004. A
904 metasomatic origin for late Archean eclogitic diamonds: Implications from internal morphology

905 of diamonds and Re-Os and S isotope characteristics of their sulfide inclusions from the late
906 Jurassic Klipspringer kimberlites. South African Journal of Geology, 107(1-2), pp.119-130.

907 Westerlund, K.J., Shirey, S.B., Richardson, S.H., Carlson, R.W., Gurney, J.J., and Harris, J.W., 2006. A
908 subduction wedge origin for Paleoarchean peridotitic diamonds and harzburgites from the
909 Panda kimberlite, Slave craton: evidence from Re-Os isotope systematics. Contributions to
910 Mineralogy and Petrology, 152, 275-294.

911 Wiggers de Vries, D.F., Pearson, D.G., Bulanova, G.P., Smelov, A.P., Pavlushin, A.D., and Davies, G.R.,
912 2013. Re-Os dating of sulphide inclusions zonally distributed in single Yakutian diamonds:
913 Evidence for multiple episodes of Proterozoic formation and protracted timescales of diamond
914 growth. Geochimica et Cosmochimica Acta, 120, 363-394.

915 Yefimova, E.S., Sobolev, N.V. and Pospelova, L.N., 1983. Vklyucheniya sul'fidov v almazakh i
916 osobennosti ikh paragenezisa. Sulfide inclusions in diamonds and their paragenesis. Zap Vses
917 Miner Obshch, 112, pp.300-310.

918

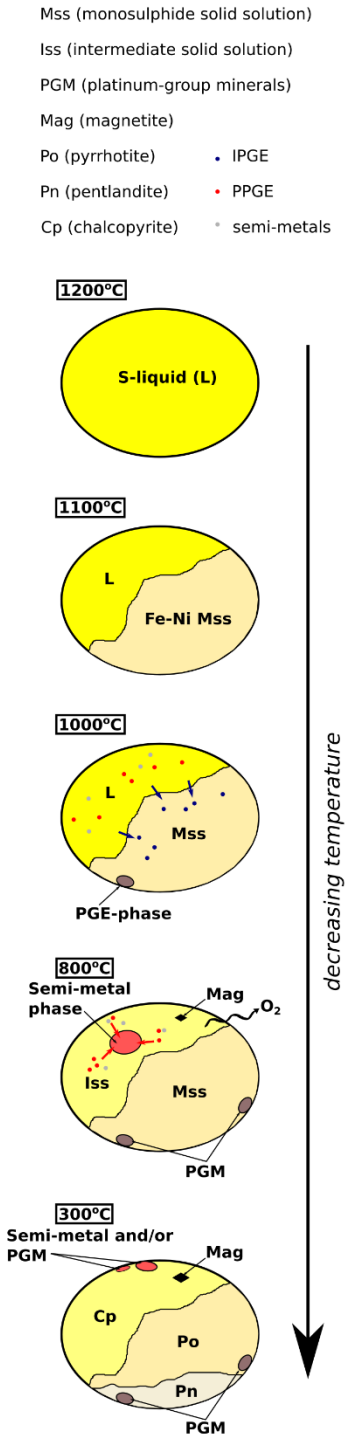

919

920 Figure 1

921

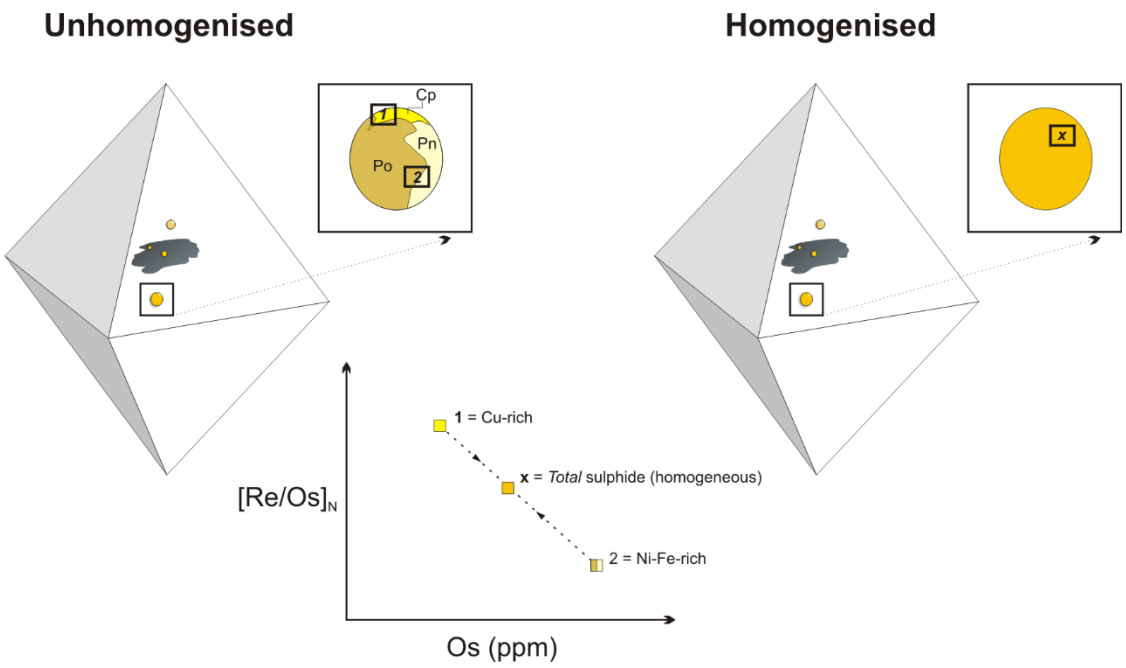

922

923 Figure 2

924

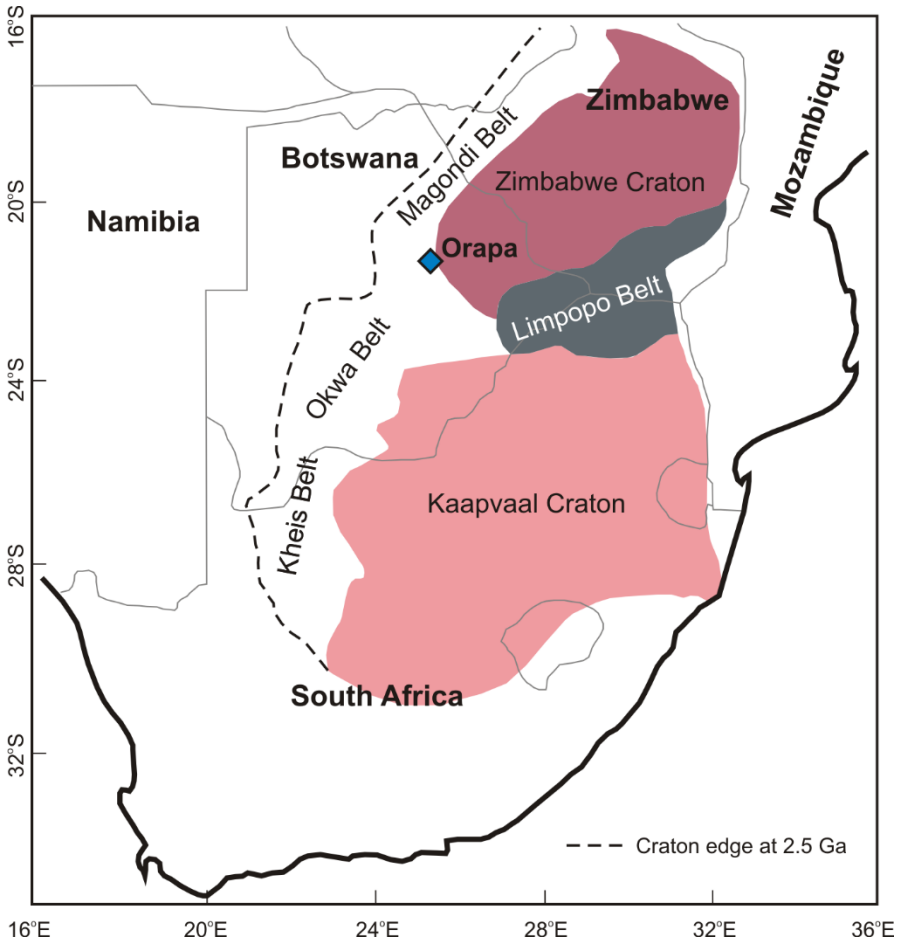

925

926 Figure 3

927

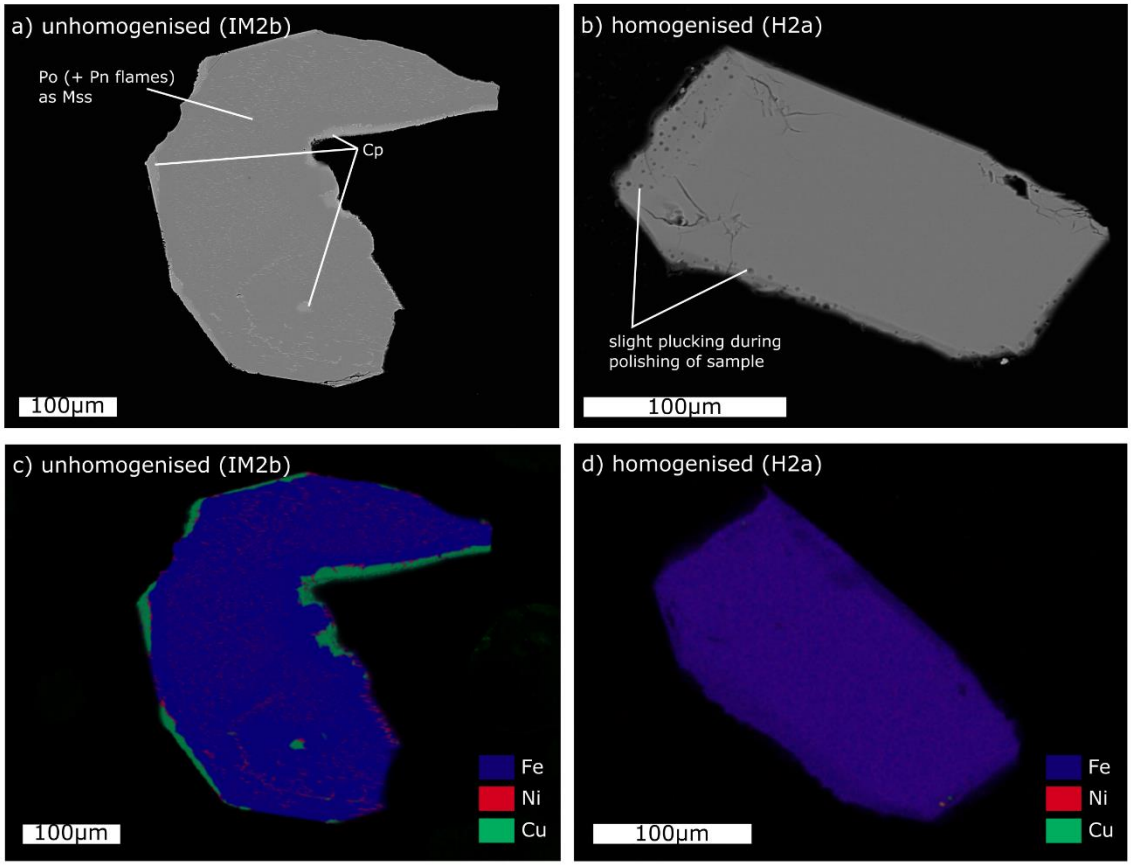

928

929 Figure 4

930

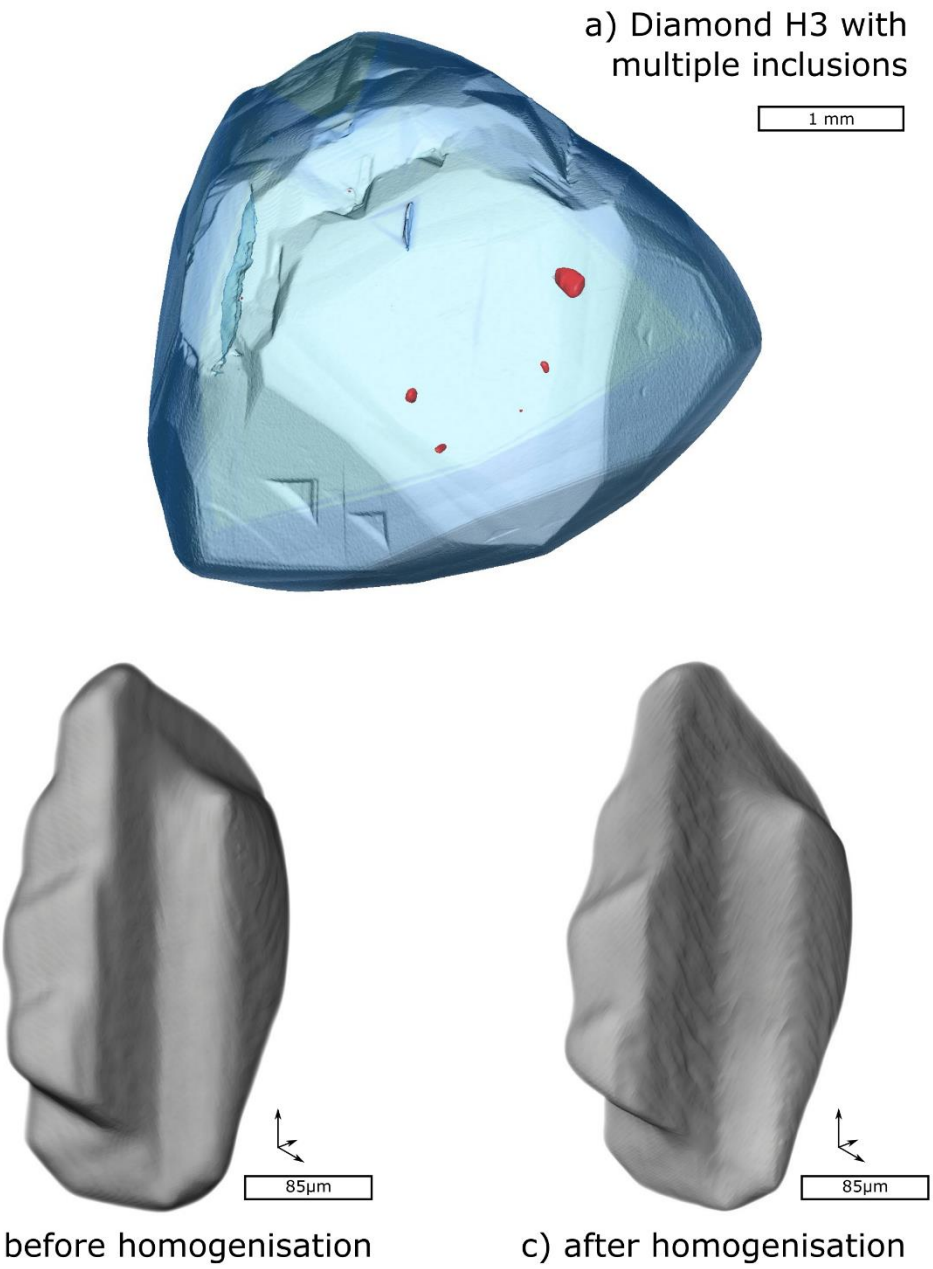

931

932 Figure 5

933

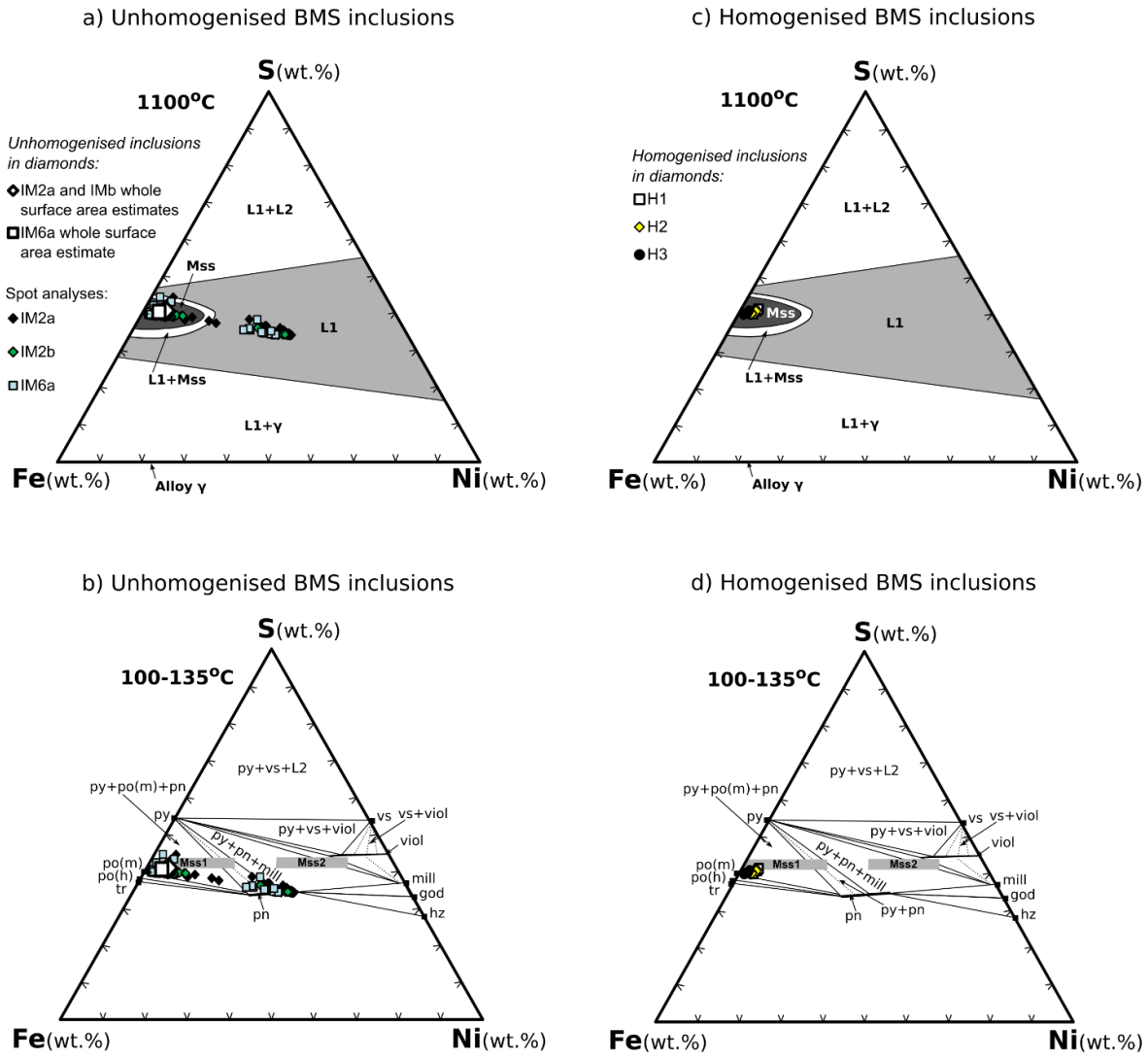

934

935 Figure 6

936

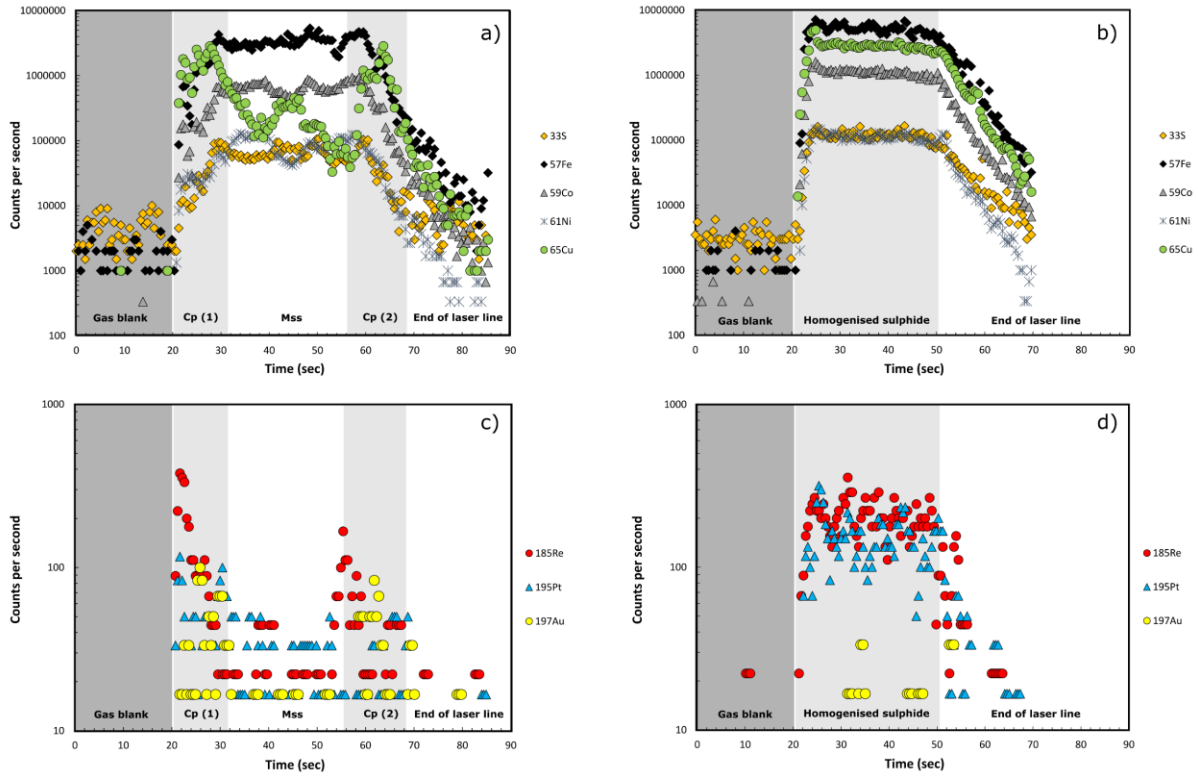

937

938 Figure 7

939

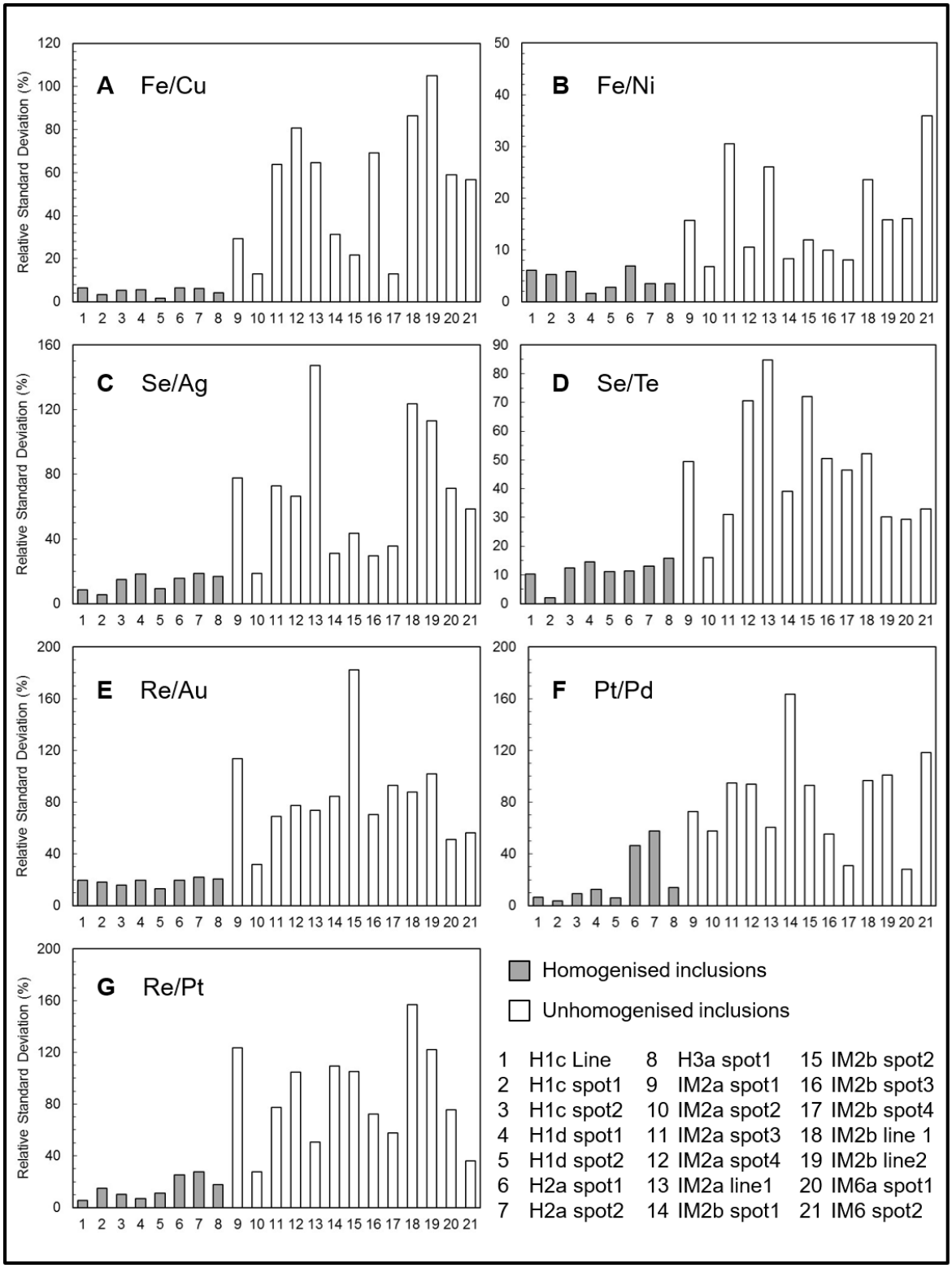
A Fe/Cu
B Fe/Ni
C Se/Ag
D Se/Te
E Re/Au
F Pt/Pd
G Re/Pt
Relative Standard Deviation (%)
Homogenised inclusions
Unhomogenised inclusions
1 H1c Line
2 H1c spot1
3 H1c spot2
4 H1d spot1
5 H1d spot2
6 H2a spot1
7 H2a spot2
8 H3a spot1
9 IM2a spot1
10 IM2a spot2
11 IM2a spot3
12 IM2a spot4
13 IM2a line1
14 IM2b spot1
15 IM2b spot2
16 IM2b spot3
17 IM2b spot4
18 IM2b line 1
19 IM2b line2
20 IM6a spot1
21 IM6 spot2

Figure 8

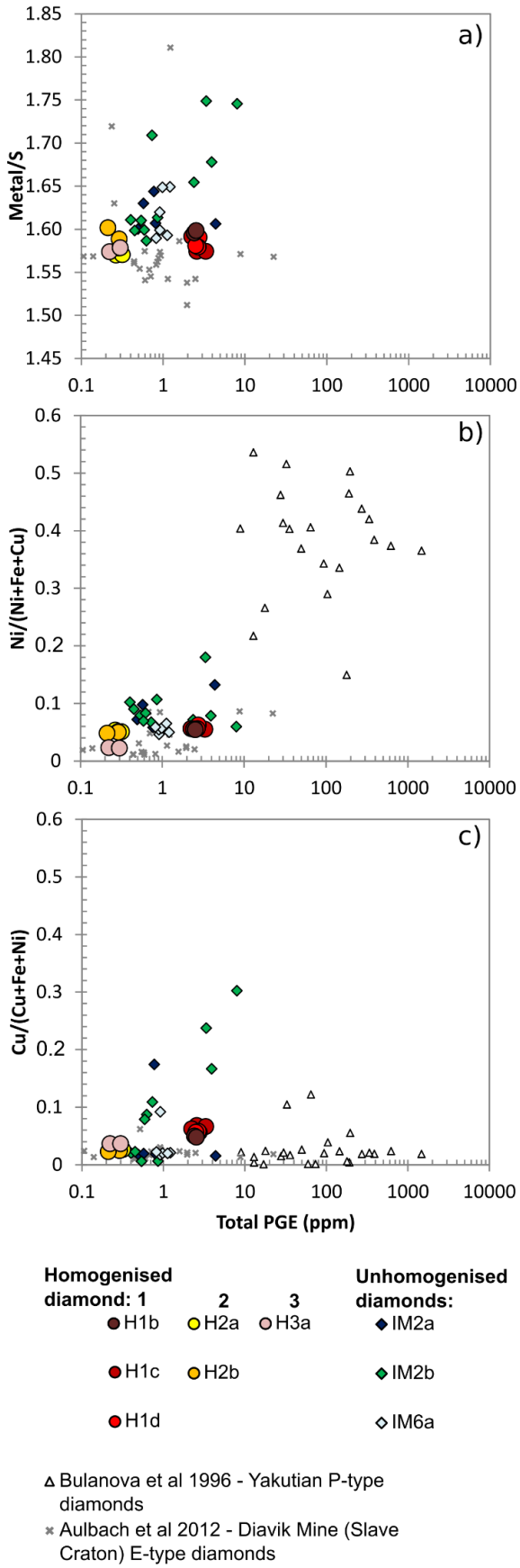

943

944 Figure 9

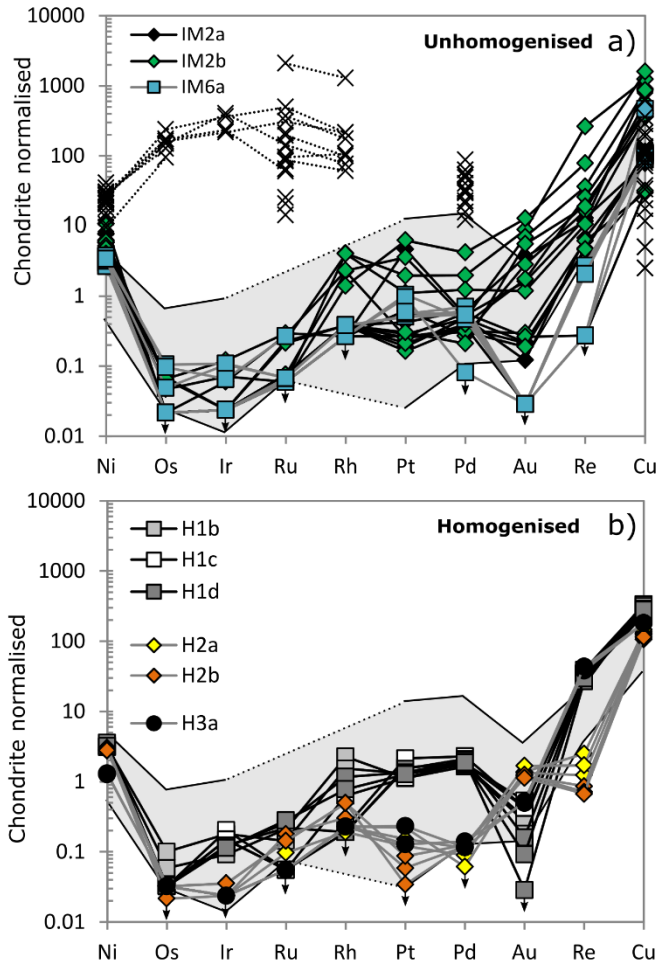

945

946 Figure 10

947

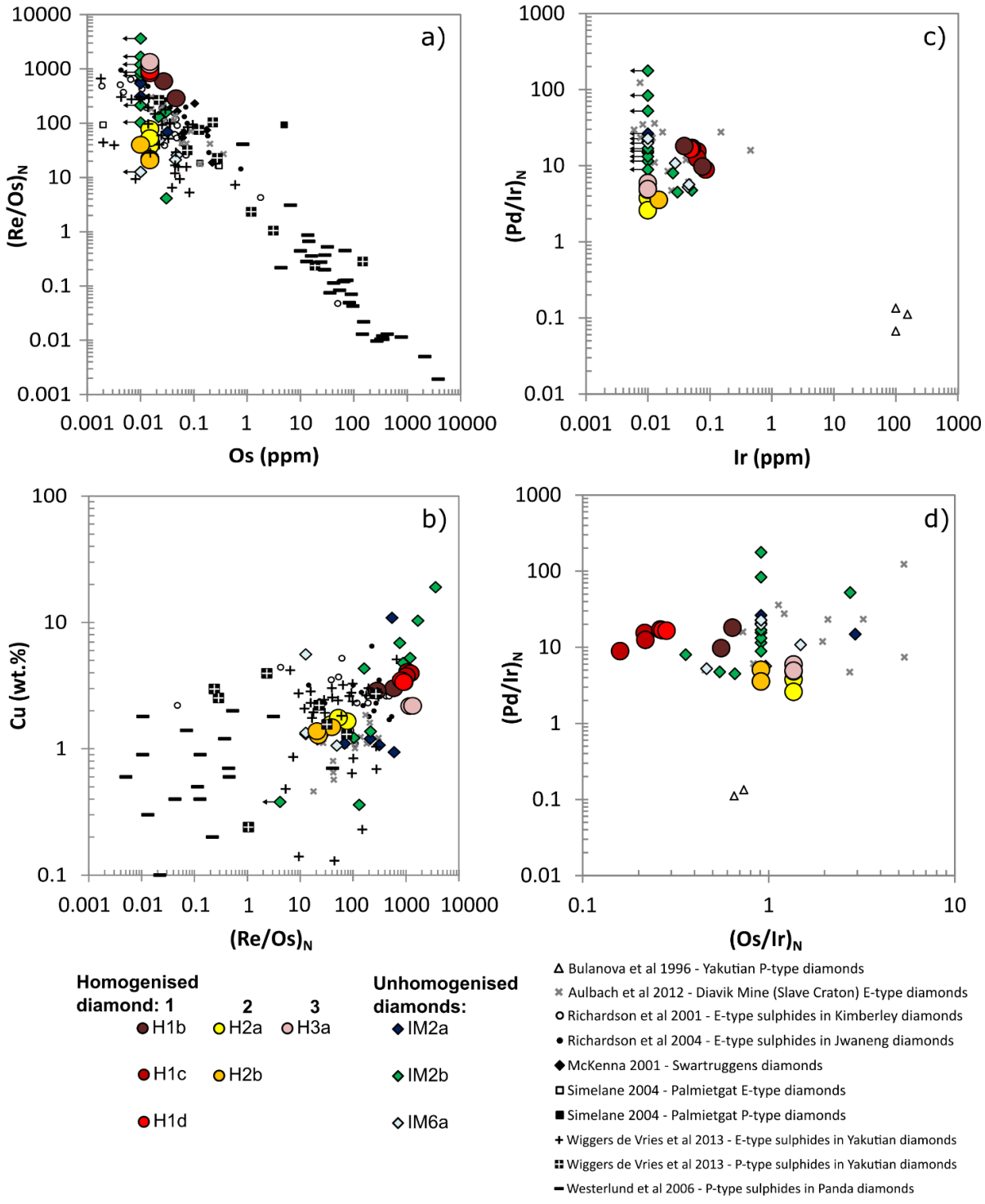

948

949 Figure 11

950

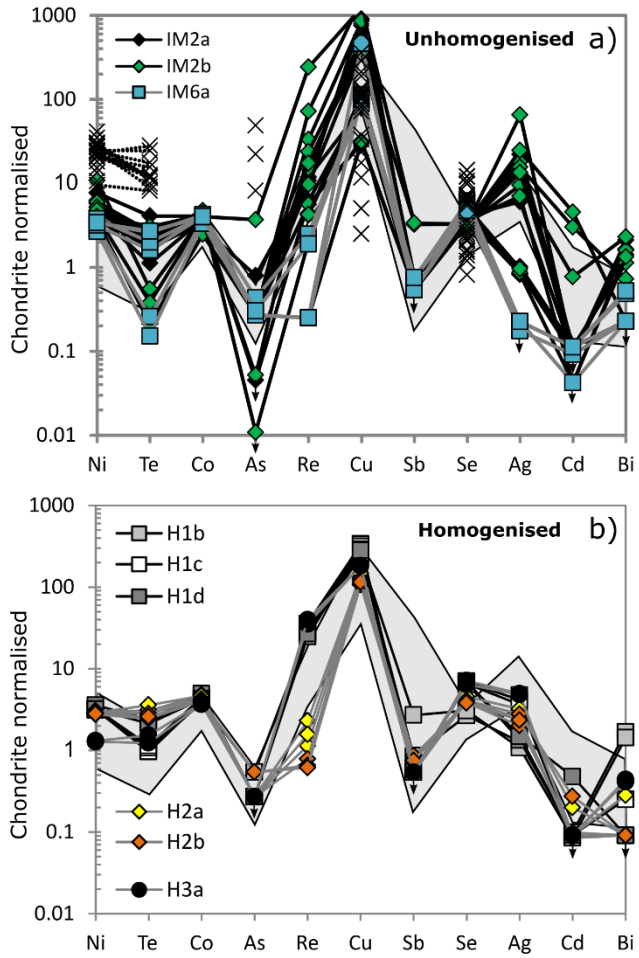

951

952 Figure 12

953

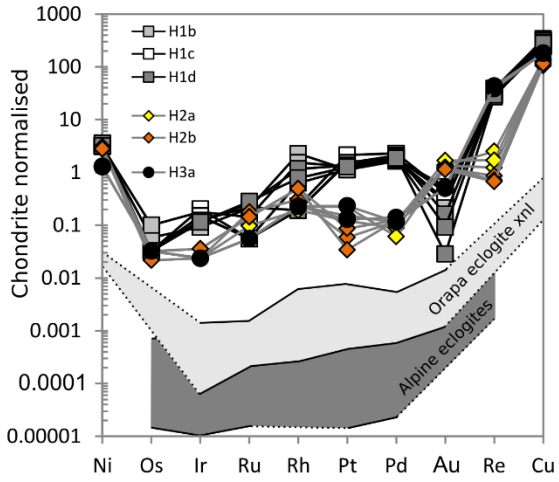

954

955 Figure 13

956

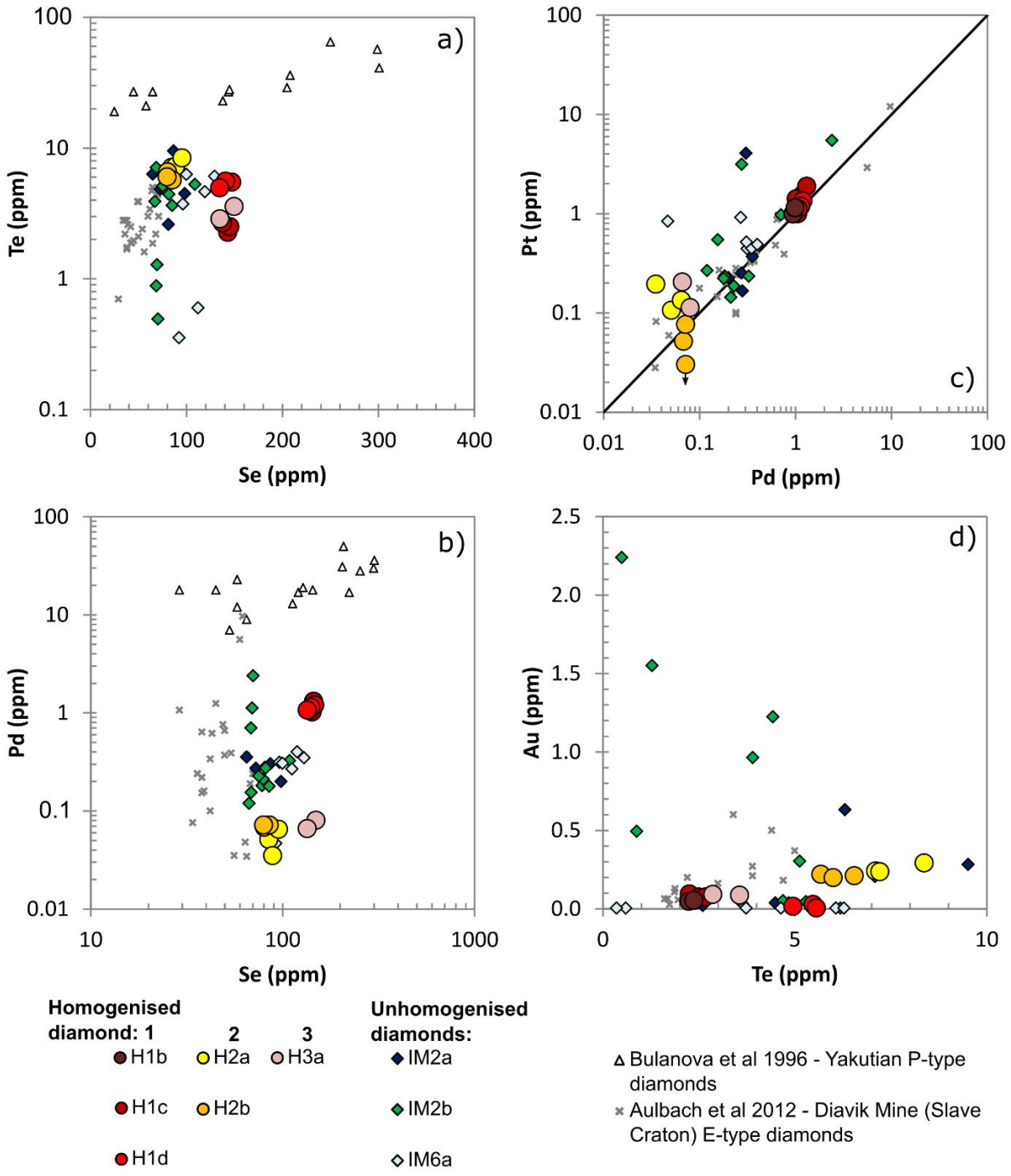

957

958 Figure 14

959

960

961

Table 1: Details of sulphide inclusions

Diamond	Sample	Dimensions (µm)	Details of fragment/inclusion	Homogenised/Unhomogenised
H1	H1a	150 x 100 x 100	Fragment from mixed multiple inclusions	Homogenised
	H1b	100 x 100 x 80	Fragment from mixed multiple inclusions	Homogenised
	H1c	100 x 100 x 80	Fragment from mixed multiple inclusions	Homogenised
	H1d	150 x 100 x 30	Fragment from mixed multiple inclusions	Homogenised
	H1e	200 x 100 x 30	Fragment from mixed multiple inclusions	Homogenised
H2	H2a	200 x 150 x 150	Whole inclusion – #1 of 4	Homogenised
	H2b	150 x 100 x 100	Whole inclusion – #2 of 4	Homogenised
H3	H3a	100 x 50 x 50	Fragment of inclusion – #1 of 5	Homogenised
IM2	IM2a	300 x 150 x 100	Fragment of single inclusion	Unhomogenised
	IM2b	350 x 300 x 250	Fragment of single inclusion	Unhomogenised
IM6	IM6a	300 x 200 x 150*	Fragment of single inclusion	Unhomogenised

** Original size of whole inclusion which subsequently broke (sample IM6a is a fragment of this original)*

962

963

964 Table 2

Sample #	Diamond #	Fragment #	Homogenised?	End-member mineral	*n*	S	Fe	Co	Ni	Cu	Total
						(wt%)					
H1a	H1	a	homogenised	n/a (mean)	*9*	38.97	53.16	0.52	3.28	3.97	99.89
				2σ		*0.15*	*0.63*	*0.04*	*0.18*	*0.34*	*0.51*
H1b	H1	b	homogenised	n/a (mean)	*3*	*38.88*	*53.50*	*0.58*	*3.32*	*3.05*	*99.33*
				2σ		*0.34*	*0.18*	*0.10*	*0.03*	*0.33*	*0.82*
H1c	H1	c	homogenised	n/a (mean)	*7*	39.00	53.03	0.50	3.21	3.87	99.60
				2σ		*0.09*	*0.37*	*0.04*	*0.10*	*0.32*	*0.29*
H1d	H1	d	homogenised	n/a (mean)	*9*	38.82	53.38	0.53	3.33	3.22	99.29
				2σ		*0.08*	*0.19*	*0.04*	*0.09*	*0.20*	*0.29*
H2a	H2	a	homogenised	n/a (mean)	*8*	39.46	54.41	0.54	3.01	1.70	99.13
				2σ		*0.29*	*0.33*	*0.03*	*0.05*	*0.06*	*0.41*
H2b	H2	b	homogenised	n/a (mean)	*4*	*39.50*	*54.32*	*0.63*	*2.97*	*1.87*	*99.29*
				2σ		*0.75*	*0.21*	*0.04*	*0.03*	*0.20*	*0.50*
H3a	H3	a	homogenised	n/a (mean)	*9*	39.08	55.93	0.50	1.40	2.19	99.09
				2σ		*0.15*	*0.30*	*0.08*	*0.04*	*0.10*	*0.37*
IM2a	IM2	a	unhomogenised	Po (mean)	*14*	39.41	56.48	0.40	3.35	0.14	99.79
				2σ		*0.52*	*3.15*	*0.33*	*3.06*	*0.06*	
				Pn (mean)	*4*	33.69	27.51	1.01	35.23	1.73	99.17
				2σ		*0.50*	*1.43*	*0.14*	*2.40*	*1.08*	
				Cp (mean)	*17*	35.35	30.99	0.14	1.23	32.62	100.33
				2σ		*0.27*	*0.74*	*0.17*	*2.21*	*2.07*	
IM2b	IM2	b	unhomogenised	Po (mean)	*10*	40.05	55.86	0.47	4.05	0.14	100.57
				2σ		*0.46*	*3.37*	*0.41*	*3.62*	*0.19*	
				Cp (mean)	*18*	35.77	30.84	0.11	0.66	32.69	100.07
				2σ		*0.39*	*1.26*	*0.09*	*1.19*	*1.14*	
IM6a	IM6	a	unhomogenised	Po (mean)	*19*	39.39	57.09	0.40	2.04	0.34	99.27
				2σ		*0.38*	*1.44*	*0.17*	*1.36*	*1.62*	
				Pn (mean)	*5*	34.83	33.64	1.22	30.41	0.54	100.63
				2σ		*1.29*	*5.60*	*0.11*	*6.45*	*0.52*	
				Cp (mean)	*13*	35.15	33.35	0.11	0.37	30.49	99.47
				2σ		*0.59*	*3.80*	*0.10*	*0.60*	*4.29*	

965

966

967

968 Table 3

Sample #		Dominant end-member BMS	LOD#	S (stoich)	S (measured)**	S/Se '	^{57}Fe	^{59}Co	^{61}Ni	^{65}Cu	^{75}As	^{77}Se	^{82}Se	^{99}Ru*	^{103}Rh*	^{105}Pd*	^{106}Pd*	^{108}Pd*	^{109}Ag	^{111}Cd	^{121}Sb	^{125}Te	^{185}Re	^{189}Os	^{193}Ir	^{195}Pt	^{197}Au	^{209}Bi
							ppm	ppm	ppm	ppm	ppm	ppm	ppm	ppm	ppm	ppm	ppm	ppm	ppm	ppm	ppm	ppm	ppm	ppm	ppm	ppm	ppm	ppm
HOMOGENISED																												
M1b	M1blinc1 ¶	n/a	1	38	38.8	6925	38.38	3076	3.41	3.06	41	-	57	0.188	0.117	0.304	1.00	0.914	0.960	0.280	<0.14	<0.24	1.30	1.80	0.028	0.040	1.01	0.049	0.169
M1b	M1bspot1 ¶	n/a	2	38	38.8	6035	38.84	1877	3.38	2.95	42	-	66	<0.22	<0.14	0.205	1.12	0.991	0.941	0.220	<0.12	0.866	2.45	1.07	0.047	0.077	1.17	0.055	0.160
	mean					6478	38.60	2027	3.38	3.01			62			0.255	1.06	0.953	0.951	0.240			2.36	1.38	0.038	0.059	1.09	0.052	0.175
	2 sd					653	0.21	70	0.04	0.09			6			0.070	0.09	0.055	0.028	0.029			0.091	0.161	0.004	0.027	0.115	0.004	0.020
M1c	M1clinc1	n/a	2	38	38.0	3726	38.76	1527	3.47	4.16	41	147	-	<0.09	<0.05	<0.05	1.04	0.965	1.15	0.855	<0.13	<0.15	2.52	1.51	<0.05	0.058	1.44	0.096	<0.02
M1c	M1cspot1	n/a	3	38	38.0	3662	38.96	1504	3.38	4.05	41	149	-	<0.09	<0.05	<0.06	1.29	1.36	1.38	0.975	<0.13	<0.15	2.57	1.47	<0.05	0.068	1.93	0.076	0.028
M1c	M1cspot2	n/a	3	38	38.0	3855	34.75	1255	3.47	3.85	41	141	-	<0.09	<0.05	0.065	1.11	1.04	1.11	0.747	<0.13	<0.15	2.74	1.34	<0.05	0.064	1.02	0.076	<0.02
	mean					3747	34.16	1222	3.43	4.02		146					1.15	1.12	1.21	0.858			2.54	1.34		0.072	1.46	0.083	
	2 sd					77	0.83	134	0.07	0.16		4					0.130	0.215	0.148	0.114			0.213	0.118		0.014	0.453	0.012	
M1d	M1dlinc1	n/a	2	38	38.2	3632	34.46	2511	3.54	5.44	41	161	-	0.155	0.149	<0.05	1.12	1.29	1.27	0.273	<0.13	<0.15	5.60	1.12	<0.05	0.053	1.37	0.029	<0.02
M1d	M1dspot1	n/a	3	38	38.2	3752	34.33	2197	3.43	5.55	41	144	-	0.177	0.150	0.156	1.16	1.13	1.20	0.309	0.146	<0.15	5.69	1.01	<0.05	0.061	1.21	<0.01	<0.02
M1d	M1dspot2	n/a	3	38	38.2	3583	34.51	2162	3.42	5.44	41	158	-	0.161	0.200	0.105	1.02	1.04	1.22	0.304	<0.13	<0.15	5.06	1.10	<0.05	0.049	1.14	0.056	<0.02
	mean					3756	34.43	2290	3.46	5.48		144		0.167	0.166	0.130	1.10	1.15	1.23	0.235			5.45	1.08		0.061	1.24	0.023	
	2 sd					135	0.09	182	0.24	0.06		7		0.022	0.022	0.027	0.08	0.128	0.058	0.020			0.339	0.062		0.002	0.115	0.009	
M2a	M2alinc1	n/a	2	38	39.6	4647	36.93	2478	3.50	1.71	41	66	-	<0.09	0.060	<0.05	0.06	<0.06	<0.09	0.510	<0.13	<0.15	7.39	0.095	<0.05	<0.02	0.110	0.349	0.052
M2a	M2aspot1	n/a	3	38	39.6	4459	37.20	2345	3.14	1.65	41	92	-	<0.09	<0.05	<0.06	<0.06	<0.06	<0.09	0.477	<0.13	<0.15	7.50	0.047	<0.05	<0.02	0.102	0.344	<0.02
M2a	M2aspot2	n/a	3	38	39.6	4125	37.30	2412	3.14	1.83	41	99	-	<0.09	<0.05	<0.06	<0.06	<0.06	0.140	0.665	0.147	<0.15	8.70	0.065	<0.05	<0.02	0.139	0.504	<0.02
	mean					4410	37.15	2377	3.19	1.72		86								0.551			7.86	0.069			0.150	0.266	
	2 sd					261	0.18	121	0.10	0.10		6								0.100			0.727	0.024			0.047	0.033	
M2b	M2blinc1 ¶	n/a	1	38	39.0	4906	38.06	2196	3.15	1.54	41	-	84	0.151	0.101	<0.06	<0.13	<0.16	<0.12	0.415	<0.14	<0.24	6.82	0.085	<0.01	<0.01	0.054	0.219	<0.02
M2b	M2bspot1 ¶	n/a	2	38	39.0	4618	38.39	2107	3.00	1.55	43	-	89	<0.22	<0.14	<0.15	<0.14	<0.13	<0.17	0.577	0.201	<0.21	5.91	0.027	<0.05	<0.05	<0.06	0.127	<0.02
M2b	M2bspot2 ¶	n/a	2	38	39.0	4945	38.79	2092	3.04	1.45	42	-	83	<0.22	<0.14	<0.13	<0.14	<0.12	<0.17	0.485	<0.12	<0.21	5.34	0.026	<0.05	<0.05	0.079	0.206	<0.02
	mean					4823	38.58	2133	3.06	1.45		85								0.492			6.02	0.028			0.066	0.217	
	2 sd					170	0.37	56	0.06	0.11		3								0.061			0.460	0.004			0.016	0.011	
M3a	M3aspot1	n/a	3	38	39.0	3609	37.84	1962	1.41	2.24	41	154	-	<0.09	<0.05	<0.06	<0.06	0.104	0.113	1.02	<0.13	<0.15	3.67	1.45	<0.05	<0.02	0.116	0.089	0.050
M3a	M3aspot2	n/a	3	38	39.0	3896	38.04	1881	1.38	2.25	41	159	-	<0.09	<0.05	<0.06	<0.06	0.127	<0.09	0.990	<0.13	<0.15	3.95	1.64	<0.05	<0.02	0.110	0.094	0.046
	mean					3753	37.94	1922	1.39	2.24		146						0.116		1.00			3.81	1.54			0.113	0.092	0.048
	2 sd					203	0.24	57	0.03	0.02		11						0.016		0.018			0.304	0.134			0.007	0.003	0.002
UNHOMOGENISED																												
IM2a	IM2alinc1	Py-Mss	2	38	n/a	4556	32.02	3055	8.06	0.94	41	57	-	<0.09	<0.06	<0.07	0.556	0.306	0.269	1.21	<0.13	<0.17	9.52	0.472	<0.02	<0.02	4.06	0.282	0.250
IM2a	IM2aspot1	Mss	3	38	n/a	4560	33.37	1873	4.37	1.07	0.1	81	-	<0.11	<0.06	<0.10	0.256	0.264	0.317	0.167	<0.16	<0.21	2.61	0.246	<0.01	<0.01	0.166	0.021	<0.05
IM2a	IM2aspot2	Py-Mss	3	38	n/a	5414	34.56	2214	5.05	1.20	41	75	-	<0.11	<0.06	<0.10	0.247	0.264	0.289	0.205	<0.16	<0.21	4.54	0.166	<0.02	<0.02	0.255	0.056	<0.05
IM2a	IM2aspot3	Mss	3	38	n/a	4009	36.25	1962	3.72	1.10	41	96	-	<0.11	<0.06	0.284	0.216	0.189	0.167	0.164	<0.06	<0.21	4.49	0.175	0.052	<0.01	0.227	0.057	0.165
IM2a	IM2aspot4	Cp-Mss	3	38	n/a	5455	47.96	1466	5.65	10.87	1.5	65	-	<0.11	<0.06	<0.10	0.396	0.316	0.550	4.59	<0.16	<0.21	6.51	0.450	<0.02	<0.02	0.570	0.652	<0.05
IM2b	IM2blinc1rim1	Cp-Py	2	38	n/a	4154	36.69	2007	11.33	14.55	7	69	-	<0.09	<0.06	0.552	1.079	1.119	1.176	15.01	<0.13	0.465	1.28	9.84	<0.02	<0.02	1.71	1.55	<0.05
IM2b	IM2blinc1core	Mss	2	38	n/a	5109	35.99	2299	4.83	0.56	41	76	-	<0.09	<0.06	<0.07	0.151	0.209	0.166	0.174	<0.13	<0.17	4.69	0.224	0.022	0.030	0.255	0.052	0.177
IM2b	IM2blinc1rim2	Mss	2	37	n/a	5557	32.09	1967	4.24	6.89	41	69	-	<0.09	<0.06	<0.07	0.206	0.155	0.123	3.60	<0.13	<0.17	0.563	0.600	<0.02	<0.02	0.546	0.494	0.180
IM2b	IM2blinc2all	Cp-Mss	2	37	n/a	5665	46.88	1732	4.67	10.33	41	82	-	0.186	0.151	0.308	0.223	0.288	0.515	3.11	2.14	<0.17	4.45	1.33	<0.02	0.025	3.14	1.22	0.080
IM2b	IM2blinc2rim1	Cp-Mss	2	38	n/a	5502	40.10	1287	3.74	18.99	41	70	-	<0.09	<0.06	0.182	2.565	2.227	2.589	4.94	2.22	<0.17	0.493	2.65	<0.02	<0.01	5.48	1.24	<0.05
IM2b	IM2blinc2core	Py-Mss	2	38	n/a	5670	34.56	2354	6.54	0.55	41	109	-	0.146	0.221	<0.07	0.551	0.282	0.548	0.191	<0.13	<0.17	5.29	<0.02	0.051	0.051	0.254	0.046	0.175
IM2b	IM2blinc2rim2	Mss	2	38	n/a	5542	34.05	2094	4.50	4.31	41	69	-	0.159	0.151	0.524	0.760	0.715	0.640	1.90	0.545	0.471	7.09	0.556	0.050	<0.02	0.971	0.206	0.255
IM2b	IM2bspot1	Py-Mss	3	38	n/a	5041	33.74	2154	6.24	1.22	41	79	-	<0.11	<0.06	<0.10	0.145	0.270	0.216	<0.09	<0.16	<0.21	6.19	0.081	<0.02	<0.02	0.145	<0.01	<0.05
IM2b	IM2bspot2	Py-Mss	3	38	n/a	4695	33.90	2165	5.46	1.37	41	85	-	<0.11	<0.06	<0.10	0.169	0.186	0.161	<0.09	<0.16	<0.21	5.64	0.169	<0.02	<0.02	0.222	0.053	0.124
IM2b	IM2bspot3	Py-Mss	3	38	n/a	5316	30.04	1762	5.00	5.24	0.1	75	-	0.116	0.166	<0.10	0.570	0.106	0.104	1.40	<0.06	<0.21	5.13	0.946	<0.02	<0.01	0.167	0.504	0.146
IM2b	IM2bspot4	Mss	3	38	n/a	5974	31.77	1725	4.22	4.78	0.6	67	-	0.149	0.119	<0.10	0.267	0.155	0.166	2.69	<0.16	<0.21	5.91	0.695	<0.02	<0.01	0.267	0.364	<0.05
IM6a	IM6alinc1all	Mss	2	38	n/a	3515	36.24	1555	3.12	1.31	41	112	-	<0.09	<0.06	<0.07	0.247	0.280	0.280	<0.07	<0.13	<0.17	0.500	<0.01	<0.01	<0.01	0.916	<0.01	<0.05
IM6a	IM6alinc1rim1	Mss	2	38	n/a	4271	32.58	1663	2.80	1.58	41	82	-	<0.09	<0.06	<0.07	<0.06	<0.06	<0.12	<0.07	<0.13	<0.17	0.554	<0.01	<0.01	<0.01	0.535	<0.01	<0.05
IM6a	IM6aspot1	Mss	3	38	n/a	4067	37.16	2082	3.33	1.06	41	96	-	<0.11	<0.06	<0.10	0.295	0.555	0.512	<0.09	<0.16	<0.21	5.73	0.066	0.025	0.044	0.442	<0.01	<0.05
IM6a	IM6aspot2	Mss	3	38	n/a	3045	37.82	2096	3.56	1.26	0.6	129	-	<0.11	<0.06	<0.10	0.560	0.299	0.566	<0.09	<0.16	<0.21	6.07	0.099	0.049	0.046	0.445	<0.01	0.055
IM6a	IM6aspot3	Mss	3	38	n/a	3502	36.59	1965	3.94	1.19	0.6	119	-	0.169	0.146	<0.10	0.426	0.427	0.545	<0.09	<0.06	<0.21	4.64	0.075	0.045	0.027	0.490	<0.01	<0.05
IM6a	IM6aspot4	Mss	3	38	n/a	3941	35.50	1995	3.55	1.34	41	100	-	<0.11	<0.06	<0.10	0.550	0.306	0.285	<0.09	<0.16	<0.21	6.26	<0.01	<0.01	<0.01	0.517	<0.01	0.057
Detection limits (LOD)																												
			1				0.01	0.206	0.01	0.00	1	17	17	0.085	0.046	0.025	0.154	0.264	0.124	0.015	0.142	0.259	0.595	0.024	0.022	0.000	0.054	0.015	0.007
			2				0.01	0.469	0.01	0.01	2	35	35	0.216	0.136	0.026	0.137	0.113	0.171	0.049	0.117	0.207	0.837	0.016	0.036	0.000	0.057	0.038	0.021
			3				0.01	0.138	0.00	0.00	3	3	3	0.075	0.044	0.015	0.060	0.082	0.027	0.045	0.231	0.080	0.607	0.024	0.023	0.000	0.054	0.008	0.008

*Denotes isotopes which have been standard-corrected (Standard 1, Cardiff University, matrix matched) for argide species and Cd.
† All results for Ru, Rh and Pd isotopes are interference corrected. See main text for details.
¶ Se concentration based on ^{82}Se isotope for these samples (as opposed to ^{77}Se for all others)
' If Cu or Ni is >5 wt.%, then Cp or Pn is noted in the dominant end-member minerals, respectively, as impeding the LA-ICPMS trace element abundances. Otherwise, Mss denoted by default.
' Calculated using measured S abundance (by SEM) and measured Se abundance (by LA-ICPMS)
- denotes 'isotope not measured'
**All homogenised samples were calibrated to measured S abundance (by SEM EDS). Given the large variation in S abundance for unhomogenised samples (due to presence of end-member BMS), unhomogenised samples were calibrated to an assumed S abundance of 38 wt.%.
This means that if the highest S concentration in a homogenised inclusion is 40 wt.%, calculated trace element concentrations would only be ~ 5% different from those based on the assumed concentration for calibration.

969

970